

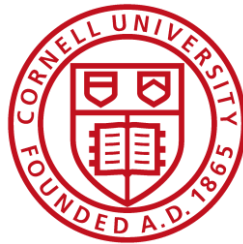
Four-Point Bending and Direct Tension Testing of Twelve Inch TR-XTREME™ Pipe Joint

Submitted to:

Russ Huggins PE
AVP of Product Development and Quality
US Pipe

By

C. Pariya-Ekkasut
H. E. Stewart
B. P. Wham
T.D. O'Rourke
C. Argyrou
T.K. Bond



Cornell University
School of Civil and Environmental Engineering
Cornell University
Hollister Hall
Ithaca, NY 14853

September, 2015

EXECUTIVE SUMMARY

US Pipe has developed a hazard resistant ductile iron (DI) pipe joint, called the TR-XTREME™ joint. Sections of 12-in. (300-mm)- diameter pipes with the new joints were tested at Cornell University to 1) evaluate the bending resistance and moment-rotation relationship of the joint for two positions of the locking clip segments, and 2) determine the capacity of the joint in direct tension. In addition, finite element (FE) analyses were performed for 4- through 16-in. (100- through 400-mm)-diameter pipelines with TR-XTREME™ joints to show how these sizes of pipelines would respond to large-scale split-basin tests, similar to the one conducted on a pipeline with 6-in. (150-mm)-diameter joints (Cornell University, 2015).

It should be noted that the term “rotation” in this report is equivalent to “deflection” as used commonly in the field and commercial pipeline information. Test results are summarized for bending and direct tension tests, as well as FE simulations under the headings that follow.

Bending Test Results

Four-point bending tests on 12-in. (300-mm)-diameter pipes were performed to evaluate the moment vs. rotation relationships of the TR-XTREME™ joints when the locking clips were at the 3 and 9 o'clock positions (Test A) and the 12 and 6 o'clock positions (Test B). Both pipes were pressurized to 80 psi (552 kPa). First leakage was observed at a moment of 565 kip-in. (63.7 kN-m) and an average joint rotation of 6.5 degrees for Test A. The leakage stopped after depressurization to approximately 60 psi (414 kPa). The pipe was repressurized to 80 psi (552 kPa) and did not leak again until a rotation of 10.3 degrees. The first leakage of Test B was detected at an applied moment of 350 kip-in. (395 kN-m) and 4.8 degrees of average joint rotation. The average rotation at first leakage for the two tests is 5.6 degrees.

The joints were able to sustain substantially higher moment and rotations beyond moment and rotation at first leakage. The maximum leakage of Test A occurred at an applied moment of 1770 kip-in. (200 kN-m) and an average joint rotation of 15.9 degrees. The test was terminated without significant damage or dislocation at the joint. The maximum leakage of Test B was observed at an applied moment of 1240 kip-in. (140 kN-m) and an average joint rotation of 11.0 degrees. The test was terminated when the restraining clips at the invert slipped out of the joint.

The moment vs. rotation relationships for the two tests are similar to a rotation of approximately 10 degrees. Higher moments were mobilized at smaller rotation angles when the clips were positioned closer to the 12 and 6 o'clock positions in alignment with the applied load. The maximum moments developed in both tests were well below both the proportional limit moment, M_{prop} , and the yield moment, M_{yield} .

Direct Joint Tension

Two tension tests were performed on the 12-in. (300-mm)-diameter US Pipe TR-XTREME™ joints. Both tests began with the spigot fully inserted in the bell. As the pipe was pressurized, the spigot was displaced from the bell seat at approximately 6 psi (41 kPa) internal pressure. The slip was 2.43 in. (61.7 mm) and 2.27 in. (57.7 mm) before the weld bead became engaged with the restraining clips for Tests 1 and 2, respectively. Tests 1 and 2 reached a maximum force of 220 kips (977 kN) at 2.83 in. (71.9 mm) of axial displacement and a maximum axial load of 259 kips (1150 kN) at 2.92 in. (74.2 mm) of joint displacement, respectively. The onset of leakage is caused by forces generated between the spigot bead and restraining clips that crack the bell circumferentially. The joints began to leak at openings of 2.84 and 2.99 in. (72.1 mm and 75.9 mm) for Tests 1 and 2, respectively. After the weld bead on the spigot made contact with the clips, an additional movement between 0.4 and 0.7 in. (10 mm and 18 mm) was required to generate leakage at the joint.

The maximum axial load of 259 kips (1150 kN) in Test 2 is more representative of the axial load capacity of the 12-in. (300-mm)-diameter US Pipe TR-XTREME™ joint and should be used for the best estimate of maximum load capacity for direct axial loading. The maximum axial load caused cracking of the pipe bell. Given an initial slip of 2.27 in. (57.7 mm) to engage contact between the spigot bead and restraining clips, an additional movement of approximately 0.65 in. (16.5 mm) was required to initiate cracking of the bell and leakage at the joint.

Finite Element Simulations

Two-dimensional (2D) finite element (FE) analyses were performed for 4-, 6-, 8-, 12-, 14-, and 16- in. (100-, 150-, 200-, 300-, 350-, and 400-mm, respectively)-diameter DI pipelines with TR-XTREME™ joints using soil, pipe, and test dimensions consistent with the large-scale split basin test performed at Cornell University for a 6-in. (150-mm)-diameter pipeline. All pipeline

dimensions used in the FE simulations are consistent with those for thickness Class 53 available from US Pipe, and the DI material properties are consistent with those of pipe commercially available from US pipe tested in previous Cornell research.

Based on the test results presented in this report, as well as previous results from large-scale Cornell tests, a scaling procedure was developed to calculate the moment vs. rotation and force vs. pullout relationships for joints with different diameters. Pipelines of 4 and 8 in. (100 and 200 mm, respectively) diameter were scaled with respect to the behavior exhibited by the 6 in. (150 mm) specimens, while pipelines of 14 and 16 in. (350 and 400 mm, respectively) were scaled relative to the results for the 12 in. (300 mm) specimen.

The FE simulation results for joint opening vs. fault displacement and joint rotation vs. fault displacement, respectively, are in close agreement for all sizes of pipe under study. They also agree very closely with those of the 6 in. (150 mm) pipeline used in the large-scale split basin test performed previously at Cornell University. The FE simulations show that the maximum axial strain distribution for each of the smaller and larger pipe size categories is the same, and is approximately $490 \mu\epsilon$ and $580 \mu\epsilon$ for 4-, 6- and 8-in. (100-, 150-, and 200-mm)-diameter pipelines and 12-, 14- and 16-in. (300-, 350-, and 400-mm)-diameter pipelines, respectively. The FE bending strains at various locations along the pipelines are provided for 9 in. (225 mm) and 18 in. (450 mm) of fault movement, and show that the bending strains increase in inverse proportion to pipe diameter. As the diameter increases, pipe segments between joints behave more like rigid pipe lengths so that the bending distortion decreases. In all cases the maximum stress from the FE results is below the DI proportional limit stress, thus indicating linear stress vs. strain behavior for all pipe sizes. The maximum axial and bending strains from the FE simulations for 6-in. (150-mm)-diameter pipe compare well with the measurements of maximum axial and bending strains obtained during the previous large-scale split basin test at Cornell, thus providing confidence in the FE results.

Significance of Large-Scale Test and Finite Element Simulation Results

The test results and FE simulations presented in this work corroborate the results of previous testing and reporting by Cornell University (2015). It should be recognized that the amount of tensile strain that can be accommodated with pipelines with TR-XTREME™ joints will depend

on the axial separation between the pipeline joints. The pipeline used in the large-scale split-basin test (Cornell University, 2015) was able to accommodate 12.2 in. (206 mm) of axial extension, corresponding to an average tensile strain of 2.61% along the pipeline. The FE results presented in this report show similar performance for all sizes of pipelines between 4 in. (100 mm) and 16 in. (400 mm). Such extension is large enough to accommodate the great majority (over 99%) of liquefaction-induced lateral ground strains measured by high resolution LiDAR after each of four major earthquakes during the recent Canterbury Earthquake Sequence (CES) in Christchurch, NZ (O'Rourke et al., 2014). These high resolution LiDAR measurements for the first time provide a comprehensive basis for quantifying ground strains caused by liquefaction on a regional basis. To put the CES ground strains in perspective, liquefaction-induced ground deformation measured in Christchurch exceed those documented in San Francisco during the 1989 Loma Prieta earthquake (e.g., O'Rourke and Pease, 1997; Pease and O'Rourke, 1997) and in the San Fernando Valley during the 1994 Northridge earthquake (e.g., O'Rourke, 1998). They are comparable to the levels of most severe liquefaction-induced ground deformation documented for the 1906 San Francisco earthquake, which caused extensive damage to the San Francisco water distribution system (e.g. O'Rourke and Pease, 1997; O'Rourke et al., 2006).

The test results and FE simulations presented in this report confirm that the TR-XTREME™ joints are able to sustain without leakage large levels of ground deformation through axial displacement and rotation. The test results are directly applicable to the performance of nominal 4-in. (100-mm) to 16-in. (400-mm)-diameter US Pipe DI pipelines with TR-XTREME™ joints.

TABLE OF CONTENTS

Executive Summary	i
Table of Contents	v
List of Figures	vi
List of Tables	viii

<u>Section</u>	<u>Page</u>
1 Introduction and Organization	1
2 Four-Point Bending Tests	2
2.1 Introduction	2
2.2 Locking Clip Locations	2
2.3 Instrumentation	4
2.4 Specimen Geometry, Material Properties, and Calculation Approaches	4
2.5 Test A Results	8
2.5.1 Pressure	8
2.5.2 Moment-Rotation	10
2.5.3 Displacements	12
2.5.4 Pipe Strains	12
2.6 Test B Results	14
2.6.1 Pressure	14
2.6.2 Moment-Rotation	16
2.6.3 Displacements	17
2.6.4 Pipe Strains	19
2.7 Conclusions for Bending Tests	19
3 Joint Tension Test	20
3.1 Introduction	20
3.2 Tension Test 1	20
3.2.1 Instrumentation	20
3.2.2 Force - Displacement	20
3.2.3 Spigot Deformations	24
3.2.4 Spigot Axial Strains	26
3.2.5 Bell Axial Strains	29
3.3 Tension Test 2	29
3.3.1 Instrumentation	29
3.3.2 Force - Displacement	29
3.3.3 Spigot Deformations	32
3.3.4 Spigot Axial Strains	35
3.3.5 Bell Axial Strains	35

TABLE OF CONTENTS (completed)

<u>Section</u>	<u>Page</u>
3.4 Test 1 and 2 Comparisons	37
3.5 Conclusions	37
4 Finite Element Simulations	39
4.1 Large-Scale Split Basin Test	39
4.2 Finite Element Simulations	41
4.3 Finite Element Simulation Results	45
4.4 Summary of Finite Element Simulations	48
5 Summary	51
References	55

LIST OF FIGURES

<u>Figure</u>	<u>Page</u>
2.1 Clip Locations Closer to 3 and 9 O’Clock for Test A	3
2.2 Clip Locations Closer to 12 and 6 O’Clock for Test B	3
2.3 Full-Scale Split Basin Test Setup with Clip Locations Closer to 12 and 6 O’Clock Positions and Lateral Ground Motion Load, P	4
2.4 Schematic of Instrumentation Locations for Bending Test A	5
2.5 Schematic of Instrumentation Locations for Bending Test B	6
2.6 Pressure vs Time for Test A	9
2.7 Final Leakage of Test A	9
2.8 Four-Point Bending Test Apparatus	10
2.9 Rotation of the Joint in Test A	11
2.10 Moment-Rotation for Test A	11
2.11 Vertical Displacements of Test A Specimen	13
2.12 Strains on Spigot and Bell Segment vs. Applied Moment in First Sequence of Test A	13
2.13 Strains on Spigot and Bell Segment vs. Applied Moment in Second Sequence of Test A	14
2.14 Pressure vs Time for Test B	15
2.15 Leakage of Test B	15
2.16 Moment-Rotation for Test B	16
2.17 Vertical Displacements of Test B Specimen	17
2.18 Strains on Spigot and Bell Segment vs. Applied Moment for Test B	18
2.19 Moment – Rotations for Tests A and B	18

LIST OF FIGURES (continued)

<u>Figure</u>	<u>Page</u>
3.1 Tension Test Layout	21
3.2 Pressure vs. Average Joint Opening of Test 1	22
3.3 Tensile Force vs. Actuator Displacement of Test 1	23
3.4 Tensile Force vs. Average Joint Opening of Test 1	23
3.5 Circumferential Crack on East Springline of Spigot of Test 1	24
3.6 Leakage of Test 1	25
3.7 Spigot Measurement Locations (Looking North)	25
3.8 Diameter Measurement Locations on Spigot Section	27
3.9 Restraining Clips Bearing Area on the Spigot of Test 1	27
3.10 Average Spigot Tensile Force vs. Spigot Axial Strain of Test 1	28
3.11 Spigot Axial Strain vs. Average Joint Opening of Test 1	28
3.12 Average Bell Tensile Force vs. Spigot Axial Strain of Test 1	28
3.13 Bell Axial Strain vs. Average Joint Opening of Test 1	28
3.14 Pressure vs. Average Joint Opening of Test 2	30
3.15 Tensile Force vs. Actuator Displacement of Test 2	31
3.16 Tensile Force vs. Average Joint Opening of Test 2	31
3.17 Leakage at Failure of Test 2 (Looking Invert)	31
3.18 Circumferential Crack on Bell Section in Test 2	33
3.19 Restraining Clips Bearing Area on the Spigot of Test 2	34
3.20 Tensile Force vs. Spigot Axial Strain of Test 2	34
3.21 Spigot Axial Strain vs. Average Joint Opening of Test 2	34
3.22 Tensile Force vs. Bell Axial Strain of Test 2	35
3.23 Bell Axial Strain vs. Average Joint Opening of Test 2	35
3.24 Pressure vs. Average Joint Opening for Tests 1 and 2	36
3.25 Tensile Force vs. Actuator Displacement for Tests 1 and 2	36
3.26 Tensile Force vs. Average Joint Opening for Tests 1 and 2	36
4.1 Plan View of Large-Scale Split Basin Test	40
4.2 2D FE Model Setup for a Pipeline under Fault Rupture	40
4.3 Normalized Moment vs. Rotation for 6 in. (150 mm) Pipe	43
4.4 Normalized Moment vs. Rotation for 12 in. (300 mm) Pipe	43
4.5 Normalized Joint Force vs. Joint Pullout for 6 in. (150 mm) Pipe	43
4.6 Normalized Joint Force vs. Joint Pullout for 12 in. (300 mm) Pipe	43
4.7 Analytical Moment vs. Rotation for 4, 6, and 8 in. (100, 150, and 200 mm) Pipes	44
4.8 Analytical Joint Force vs. Joint Pullout for 4, 6, and 8 in. (100, 150, and 200 mm) Pipes	44

LIST OF FIGURES (completed)

<u>Figure</u>		<u>Page</u>
4.9	Analytical Moment vs. Rotation for 12, 14, and 16 in. (300, 350, and 400 mm) Pipes	44
4.10	Analytical Joint Force vs. Joint Pullout for 12, 14, and 16 in. (300, 350, and 400 mm) Pipes	44
4.11	Joint Opening vs. Fault Displacement for 6 in. (150mm) Pipes	46
4.12	Joint Rotation vs. Fault Displacement for 6 in. (150mm) Pipes	46
4.13	Joint Opening vs. Fault Displacement for 12 in. (300mm) Pipes	46
4.14	Joint Rotation vs. Fault Displacement for 12 in. (300mm) Pipes	46
4.15	Axial Strain Comparisons at 9 in. (229 mm) of Fault Displacement	47
4.16	Axial Strain Comparisons at 18 in. (457 mm) of Fault Displacement	47
4.17	Bending Strain Comparisons at 9 in. (229 mm) of Fault Displacement	47
4.18	Bending Strain Comparisons at 18 in. (457 mm) of Fault Displacement	47

LIST OF TABLES

<u>Table</u>		<u>Page</u>
2.1	Instrumentation for US Pipe TR-XTREME™ Bending Test A	5
2.2	Instrumentation for US Pipe TR-XTREME™ Bending Test B	6
2.3	Geometric and Material Properties for Bending Test Specimens	7
3.1	Instrumentation for US Pipe TR-XTREME™ Joint Tension Test 1	21
3.2	Diameter Measurements on Spigot Section for Test 1	26
3.3	Instrumentation for US Pipe TR-XTREME™ Joint Tension Test 2	30
3.4	Diameter Measurements on Spigot Section for Test 2	32
4.1	Summary of Maximum Strains and Stresses for 4 to 16 in. Pipes	49

Section 1

Introduction and Organization

This report presents testing results performed at Cornell University for 12-in. (300-mm)-diameter ductile iron (DI) pipe with a new hazard-resistant joint designed by US Pipe. The purpose of the testing was to characterize the mechanical behavior of the TR-XTREME™ jointed pipe under four-point bending and direct tension loading. The report is organized in five sections, the first of which provides introductory remarks and describes the report organization. Section 2 presents the results of two four-point bending tests performed to determine the moment-rotation relationships and leakage thresholds of the joints. Section 3 presents the results of two direct tension tests performed to evaluate the axial force vs displacement characteristics and associated leakage thresholds for this type of loading. Section 4 summarizes the results of finite element analyses of 4-, 6-, 8-, 12-, 14-, and 16-in. (100-,150-,200-,300-,350-, and 400-mm) pipelines with TR-XTREME™ joints to show how these sizes of pipelines would respond to large-scale split-basin tests. Section 5 provides summary remarks and draws conclusions for the testing. It should be noted that the term “rotation” in this report is equivalent to “deflection” as used commonly in the field and commercial pipeline information.

Section 2

Four-Point Bending Tests

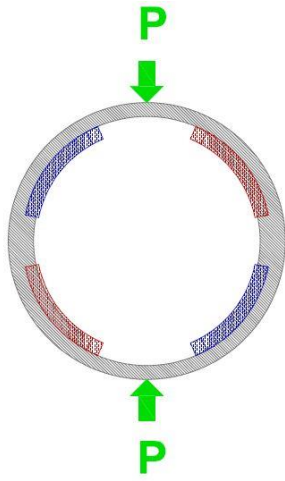
2.1 Introduction

This report describes two four-point bending tests on 12-in. (300 mm) ductile iron (DI) joint specimens provided by US Pipe. The test results are used to determine the moment-rotation response of the newly designed TR-XTREME™ bell and spigot pipe sections. Of particular interest was the effect that the location of the locking ring segments had on the rotational response. In this report the special locking segments are referred to as clips.

2.2 Locking Clip Locations

During the four-point bending tests the load, P , is applied vertically. For the first test, Test A, the slot was positioned at the top of the pipe and the locking clips were inserted such that they were located near the springline of the pipe, as shown schematically in Figure 2.1 a). Figure 2.1 b) shows a photograph of the clips in position near the springline. Specimen B was rotated 90 degrees from the orientation of Test A, such that its slots were located at the springline of the pipe and the locking clips were near the crown and invert of the pipe, as shown in Figure 2.2 a). Figure 2.2 b) presents a photograph of the clips in position near the pipe crown and invert. Under the assumption that the slots are at the springline during regular pipeline installation, the vertical load applied to the pipe for Test A is representative of lateral load generated by horizontal differential soil displacement. Horizontal soil displacement is typically associated with the most severe conditions of soil-pipe interaction during earthquake induced ground deformation.

During typical installation, as well as in the full-scale split basin simulations, the 12 in. (150 mm) pipeline is constructed with the slots at the springline and locking clips near the 12 and 6 o'clock positions as shown in Figure 2.3. The orientation of the clips is the same as that in Figure 2.2, but the load, P , from the soil is applied laterally. Therefore, the first 4-pt bending test (Test A) is representative of the rotational behavior of the joint under lateral loading, such as the deformation imposed during the split basin test.

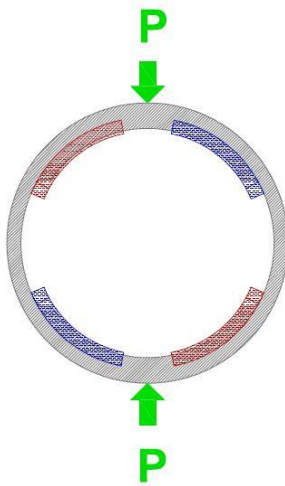


a) Schematic



b) Photo

Figure 2.1. Clip Locations Closer to 3 and 9 O'Clock for Test A

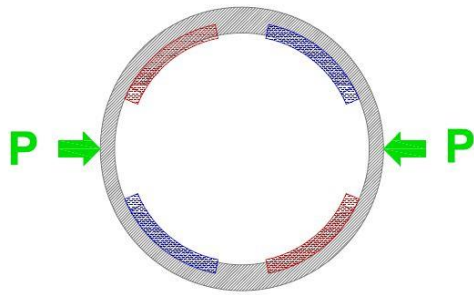


a) Schematic



b) Photo

Figure 2.2. Clip Locations Closer to 12 and 6 O'Clock for Test B



a) Schematic



b) Photo

Figure 2.3. Full-Scale Split Basin Test Setup with Clip Locations Closer to 12 and 6 O’Clock Positions and Lateral Ground Motion Load, P

2.3 Instrumentation

A variety of instrumentation was used in the bending tests. Figures 2.4 and 2.5 show schematics of the test setup for Test A and Test B, respectively. Although the center of rotation for the complex inner geometry of the bell and its interaction with the weld bead connection is not well defined, the joint was positioned such that the vertical load was applied at the nominal center of the bell and spigot specimen. Before bending, the spigot end was inserted fully into the bell for a depth of insertion of 2.70 in. (68.6 mm). Tables 2.1 and 2.2 list the instrumentation locations, types of instrument, and local instrument names used for both tests.

2.4 Specimen Geometry, Material Properties, and Calculation Approaches

Table 2.3 presents the geometric and material properties for the ductile iron pipe used in the bending tests. The yield stress, $\sigma_y = 45.1$ ksi (311 MPa), is based on the tensile test data from commercially available ductile iron reported by Wham and O’Rourke (2015). The proportional limit stress, $\sigma_{prop} = 39.5$ ksi (272 MPa), is the stress near the end of the elastic range, as determined from the tensile coupon test data.

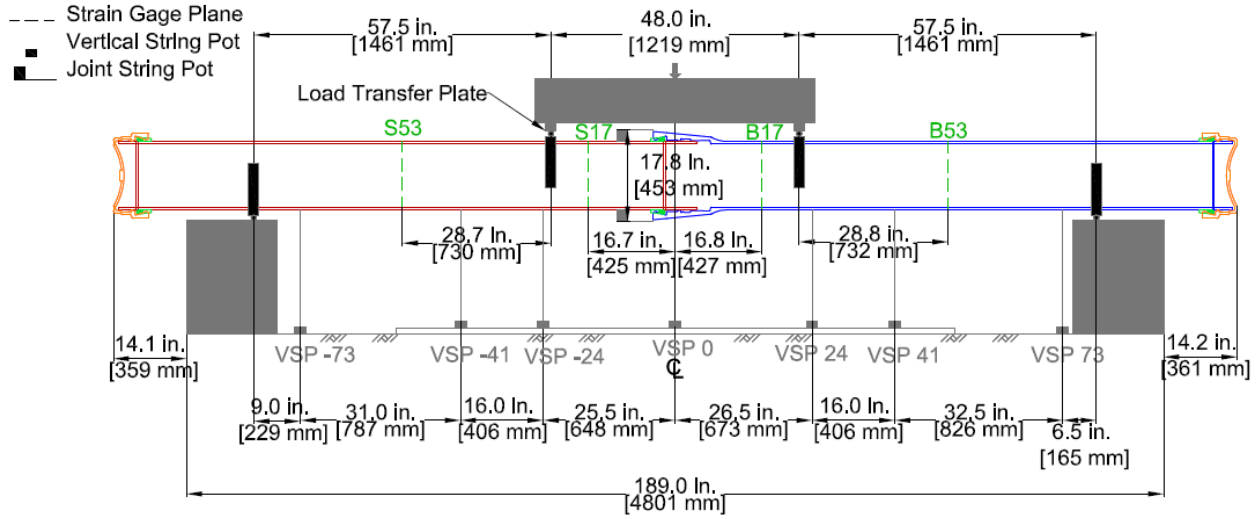


Figure 2.4. Schematic of Instrumentation Locations for Bending Test A

Table 2.1. Instrumentation for US Pipe TR-XTREME™ Bending Test A

Location	Instrument	Local Instrument Name
72.5 in. from Joint	Vertical String Pot on Spigot End	VSP-73
41.5 in. from Joint	Vertical String Pot on Spigot End	VSP-41
25.5 in. from Joint	Vertical String Pot on Spigot End	VSP-24
Top of Bell	Horizontal String Pot	HSP Top
Bottom of Bell	Horizontal String Pot	HSP Bot
0 in. from Joint	Vertical String Pot on Bell End	VSP 0
26.5 in. from Joint	Vertical String Pot on Bell End	VSP 24
42.5 in. from Joint	Vertical String Pot on Bell End	VSP 41
75.0 in. from Joint	Vertical String Pot on Bell End	VSP 73
52.7 in. from Joint	Strain Gage at Crown on Spigot End	S53C
52.7 in. from Joint	Strain Gage at Invert on Spigot End	S53I
16.7 in. from Joint	Strain Gage at Crown on Spigot End	S17C
16.7 in. from Joint	Strain Gage at Invert on Spigot End	S17I
16.7 in. from Joint	Strain Gage at Spingline on Spigot End	S17F
16.7 in. from Joint	Strain Gage at Spingline on Spigot End	S17B
16.8 in. from Joint	Strain Gage at Crown on Bell End	B17C
16.8 in. from Joint	Strain Gage at Invert on Bell End	B17I
16.8 in. from Joint	Strain Gage at Spingline on Bell End	B17F
16.8 in. from Joint	Strain Gage at Spingline on Bell End	B17B
52.8 in. from Joint	Strain Gage at Crown on Bell End	B53C
52.8 in. from Joint	Strain Gage at Invert on Bell End	B53I
Center of Load	Load Cell	Load
Bell End	Pressure Gage	Pressure

1 in. = 25.4 mm

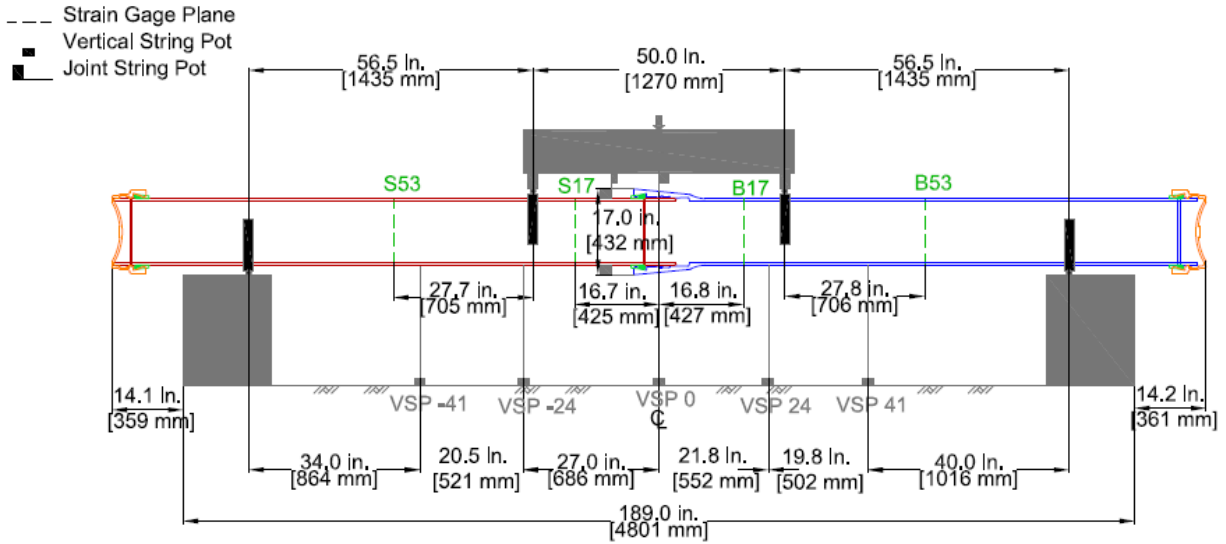


Figure 2.5. Schematic of Instrumentation Locations for Bending Test B

Table 2.2. Instrumentation for US Pipe TR-XTREME™ Bending Test B

Location	Instrument	Local Instrument Name
47.5 in. from Joint	Vertical String Pot on Spigot End	VSP-41
27 in. from Joint	Vertical String Pot on Spigot End	VSP-24
Top of Bell	Horizontal String Pot	HSP Top
Bottom of Bell	Horizontal String Pot	HSP Bot
0 in. from Joint	Vertical String Pot on Bell End	VSP 0
21.8 in. from Joint	Vertical String Pot on Bell End	VSP 24
41.6 in. from Joint	Vertical String Pot on Bell End	VSP 41
52.7 in. from Joint	Strain Gage at Crown on Spigot End	S53C
52.7 in. from Joint	Strain Gage at Invert on Spigot End	S53I
16.7 in. from Joint	Strain Gage at Crown on Spigot End	S17C
16.7 in. from Joint	Strain Gage at Invert on Spigot End	S17I
16.7 in. from Joint	Strain Gage at Spingline on Spigot End	S17F
16.7 in. from Joint	Strain Gage at Spingline on Spigot End	S17B
16.8 in. from Joint	Strain Gage at Crown on Bell End	B17C
16.8 in. from Joint	Strain Gage at Invert on Bell End	B17I
16.8 in. from Joint	Strain Gage at Spingline on Bell End	B17F
16.8 in. from Joint	Strain Gage at Spingline on Bell End	B17B
52.8 in. from Joint	Strain Gage at Crown on Bell End	B53C
52.8 in. from Joint	Strain Gage at Invert on Bell End	B53I
Center of Load	Load Cell	Load
Bell End	Pressure Gage	Pressure

1 in. = 25.4 mm

Table 2.3. Geometric and Material Properties for Bending Test Specimens

Property	Value
Outside Diameter, D_o (in.)	13.13
Inside Diameter, D_i (in.)	12.3
Wall Thickness, t (in.)	0.415
Distance to Outer Fiber, c (in.)	6.57
Moment of Inertia, I (in. ⁴)	335
Proportional Limit Stress, σ_{prop} (ksi)	39.5
Yield Stress, σ_y (ksi)	45.1
M_{prop} (kip-in.)	2020
M_y (kip-in.)	2300

1 in. = 25.4 mm; 1 ksi = 6.89 MPa; 1 kip-in. = 0.113 kN-m

The outer fiber stress due to bending, σ_b , is calculated as

$$\sigma_b = \frac{M c}{I} \quad (2.1)$$

where M is moment, c is outside pipe radius, and I is moment of inertia. Thus, using the stress limits given in Table 2.3, the moment at the proportional limit, M_{prop} , and the moment at the yield stress, M_y , are as given in Table 2.3.

The length of the test specimens between the outer supports was 163 in. (4140 mm). The central 48-in. (1220 mm) span had equal lengths of 57.5 in. (1.46 m) on each side, as shown in Figure 2.4.

The moment applied to the central portion of the specimen, $M_{central}$, was calculated as

$$M_{central} = \frac{P}{2} \ell_{central} \quad (2.2)$$

where P is the applied load, and $\ell_{central}$ is the distance from the support to the central zone, or moment arm, of 57.5 in. (1.46 m). Moments outside the central zone (e.g. gage planes B53 and S53) have moment arms of 28.75 in. (0.73 m).

Two methods were used to calculate joint rotations. One method uses the horizontal string pots (HSPs) at the top and bottom of the bell and their vertical separation distances to calculate the joint rotation. Equation 2.3 gives the method used to evaluate the joint rotation, θ , as:

$$\theta \text{ (degrees)} = \tan^{-1} \left[\frac{\text{(top disp.-bottom disp.)}}{\text{distance between centers of HSPs} = 17.8 \text{ in}} \frac{180^\circ}{\pi} \right] \quad (2.3)$$

An alternate approach is to take the difference between the string pot measurement at the specimen center and the closest bell or spigot pot, and divide by the pot separation distance. The arctangent of this is the rotation of each side. This is given in Eq. 2.4. The overall joint rotation is the sum of the two side angles. For example,

$$\theta \text{ (degrees)} = \tan^{-1} \left(\frac{\text{(VSP 0)in.} - \text{(VSP-24)in.}}{25.5 \text{ in.}} \right) + \tan^{-1} \left(\frac{\text{(VSP 0)in.} - \text{(VSP 24)in.}}{26.5 \text{ in.}} \right) \quad (2.4)$$

where (VSP 0), (VSP-24), and (VSP 24) are the vertical string pot measurements at the string pots listed in Tables 2.1 and 2.2.

2.5 Test A Results

2.5.1 Pressure

Test A was pressurized with water to approximately 82 psi (565 kPa). The line transmitting water pressure was open for the duration of the test. Figure 2.6 shows the pressure plotted against time. When leakage (about 150 ml/min) was first observed, the pressurizing line was closed. The pressure dropped to approximately 64 psi (441 kPa). Because the leakage stopped a few seconds after closing the pressurizing line, the pipe was repressurized. As shown in the figure, the internal pressure returned to approximately 82 psi (565 kPa) with no additional leakage, and the test was continued. The second leakage of 3 ml/min was observed at approximately 1900 seconds, after which pipe loading continued. At about 2100 seconds, the load transfer plate broke (see Figure 2.4). The pressure line was turned off, and the leakage stopped at a pressure of about 68 psi (469 kPa). The test was then paused, ending the first sequence of the test.

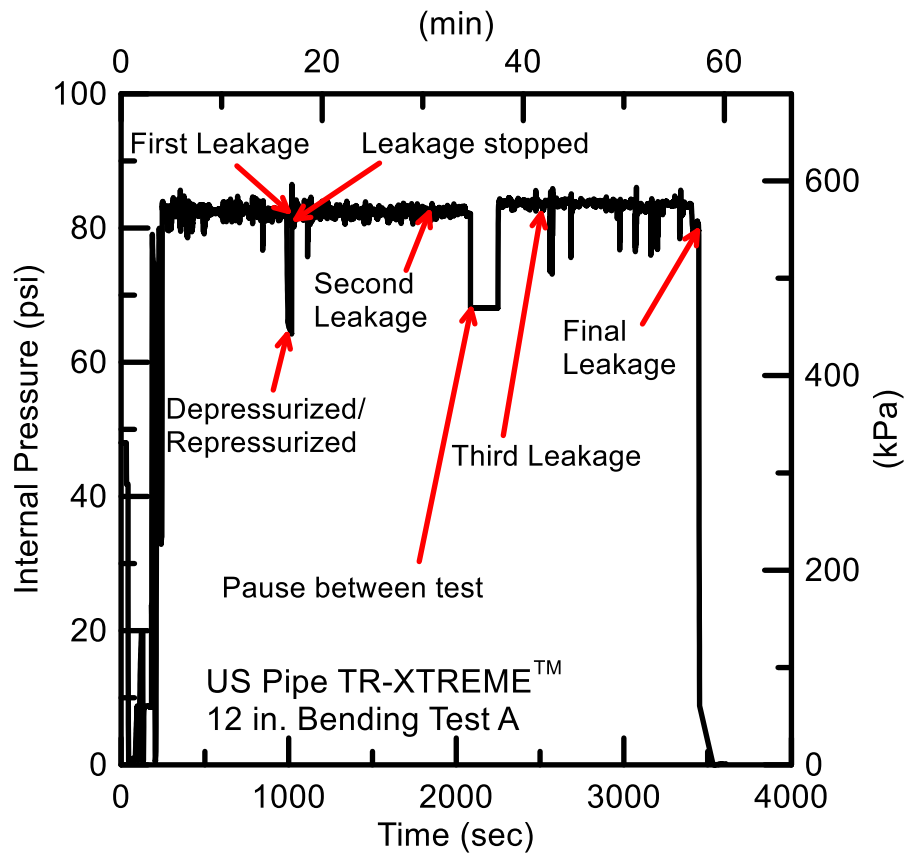


Figure 2.6. Pressure vs. Time for Test A



Figure 2.7. Final Leakage of Test A



Figure 2.8. Four-Point Bending Test Apparatus

After a new load transfer plate was inserted, the second sequence of the test began. Leakage was observed again at a rate of 3 ml/min at 2500 seconds. The rate of leakage increased as the pipe continued to be loaded. The test was stopped when the leakage reached 33 liters per minute. Figure 2.7 shows the leakage at the end of the test.

2.5.2 Moment-Rotation

Figure 2.8 is a photograph of the bending test setup showing the two steel rocker supports of the pipe (labeled A). The central load was applied through a steel beam (labeled B) in the photo. The load was applied using a 400 kip (1780 kN) Baldwin testing device.

Figure 2.9 shows the joint rotation in Test A. Joint rotations for Test A at the central portion of the bell and spigot joint were calculated using a) the horizontal string pots (HSPs) at the top and bottom of the bell (Eqn. 2.3) and b) the three vertical string pots (VSPs) in the central portion (Eqn. 2.4). Figure 2.10 shows the moment-rotation data using both approaches. The moments are those in the central load pipe section, as determined by Equation 2.2. Both measurement methods are in good agreement. The applied moments are well below the proportional limit of

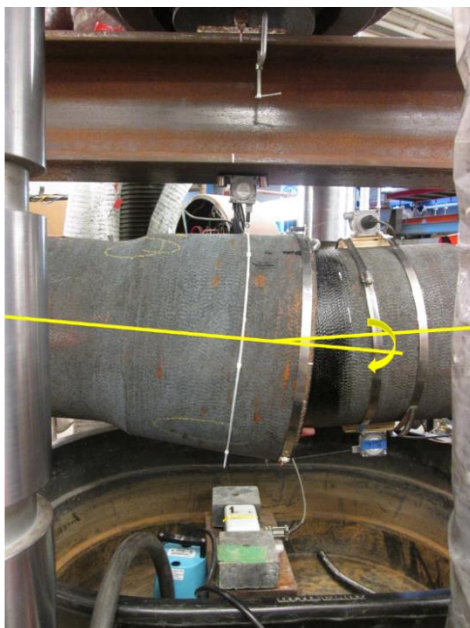


Figure 2.9. Rotation of the Joint in Test A

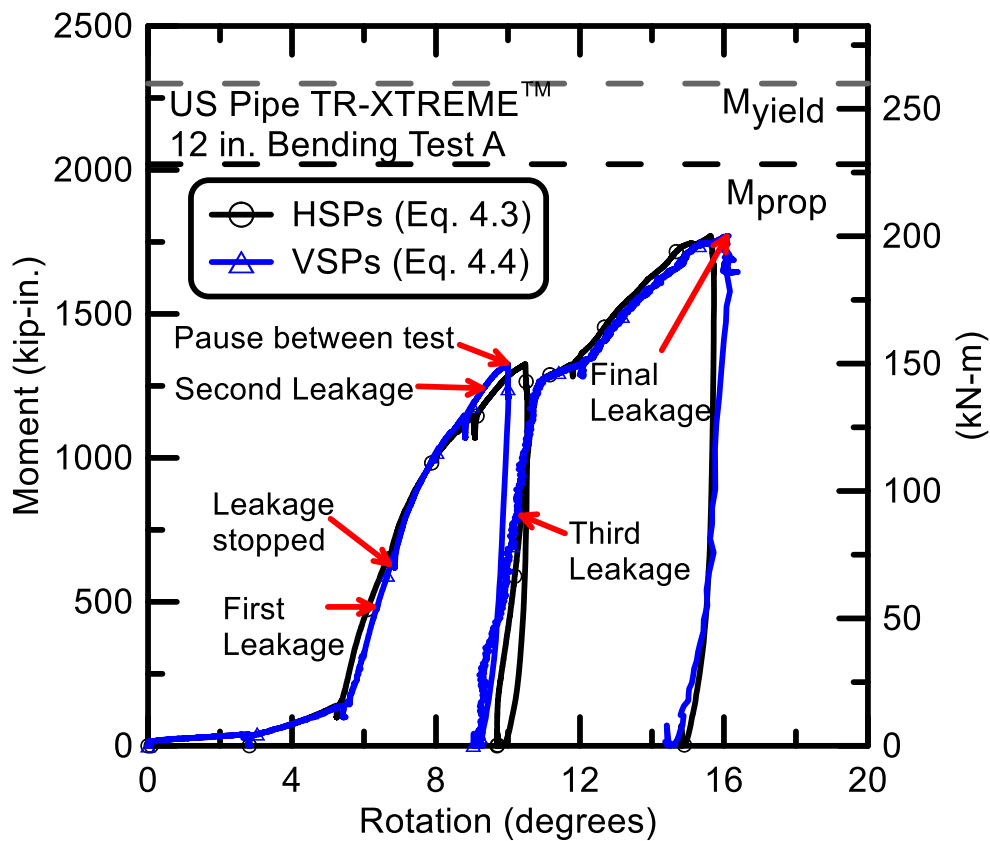


Figure 2.10. Moment-Rotation for Test A

$M_{prop} = 2020$ kip-in. (228 kN-m) based on a proportion limit stress of $\sigma_{PL} = 39.5$ ksi (272 MPa). They are also well below the yield limit, $M_y = 2300$ kip-in. (260 kN-m) based on the yield stress of $\sigma_y = 45.1$ ksi (311 MPa), as calculated from Equation 2.1.

First leakage (150 ml/min) was observed at a moment of 565 kip-in. (63.7 kN-m) and an average joint rotation of 6.5 degrees (Eqns. 2.3 and 2.4). As previously stated, the pipe was depressurized, and the leakage stopped. The pipe was repressurized, and leakage (3 ml/min) was observed again at 1210 kip-in. (137 kN-m) and an average rotation of 10.3 degrees. After the test was resumed with a new loading plate, leakage (3 ml/min) was observed at 635 kip-in. (71.6 kN-m) and an average rotation of 10.1 degrees. The rate of leakage increased as the test continued. Final leakage of 33 l/min was observed at 1770 kip-in. (200 kN-m) and an average rotation of 15.9 degrees.

2.5.3 Displacements

Pipe vertical displacements were measured at several distances along the pipe using VSPs. Figure 2.11 shows the VSP readings at these distances. In the figure positive distances along the x-axis represent the bell portion of the pipe and negative values from the load centerline represent the spigot portion. The displacements increased as the load increased, until the specimen failed at a load of approximately 64 kips (285 kN). The displacements are symmetric about the load centerline and show a linear variation with distance. This validates the assumption of rigid body rotation so that the calculation of rotation can be made from the VSP measurements.

2.5.4 Pipe Strains

Axial strains at the crown and invert vs. moment for the first and second sequences of loading during Test A are shown in Figures 2.12 and 2.13, respectively. The strains decrease with distance from the pipe joint. The spigot strains at all gage planes are nearly the same for equal applied moments. However, the bell strains outside the central load pipe section are slightly greater than those inside the central section for equal applied moments. In addition, the spigot strains are generally greater than the bell strains for the same applied moments.

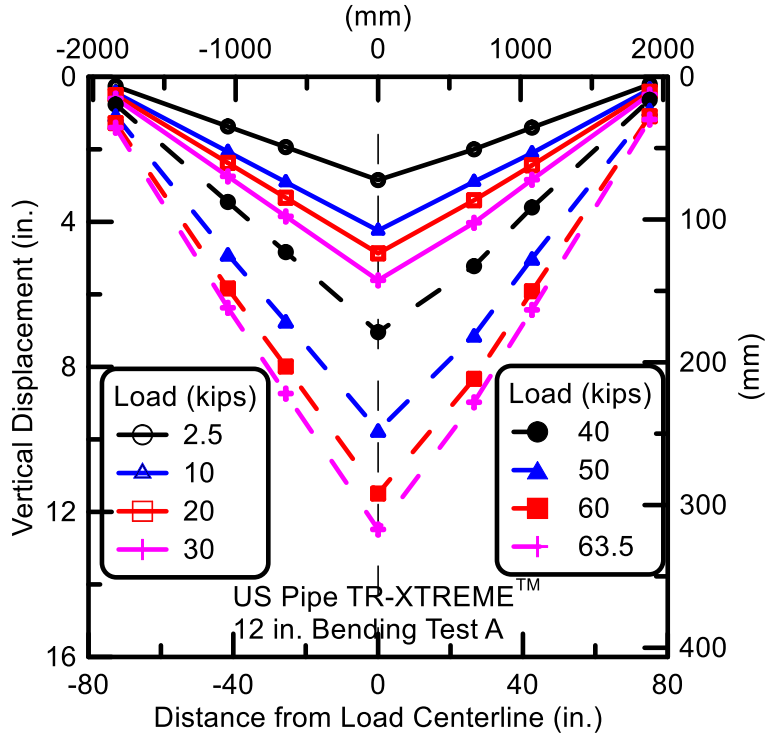
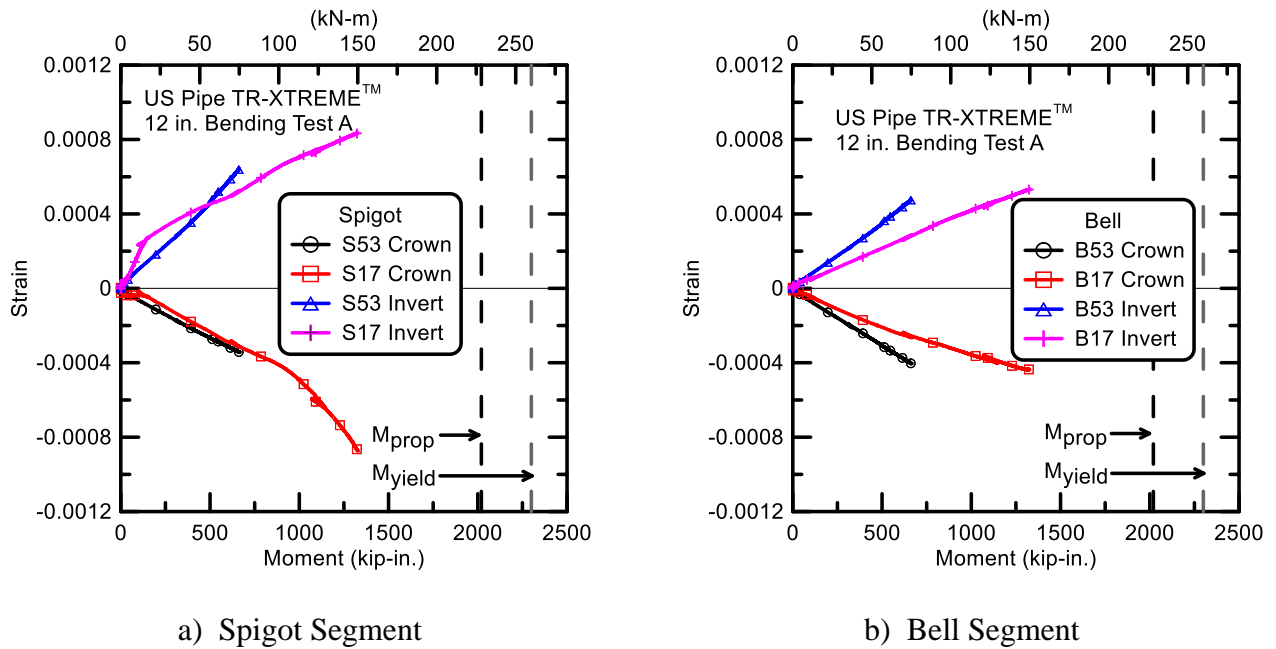


Figure 2.11. Vertical Displacements of Test A Specimen



a) Spigot Segment

b) Bell Segment

Figure 2.12. Strains on Spigot and Bell Segment vs. Applied Moment in First Sequence of Test A

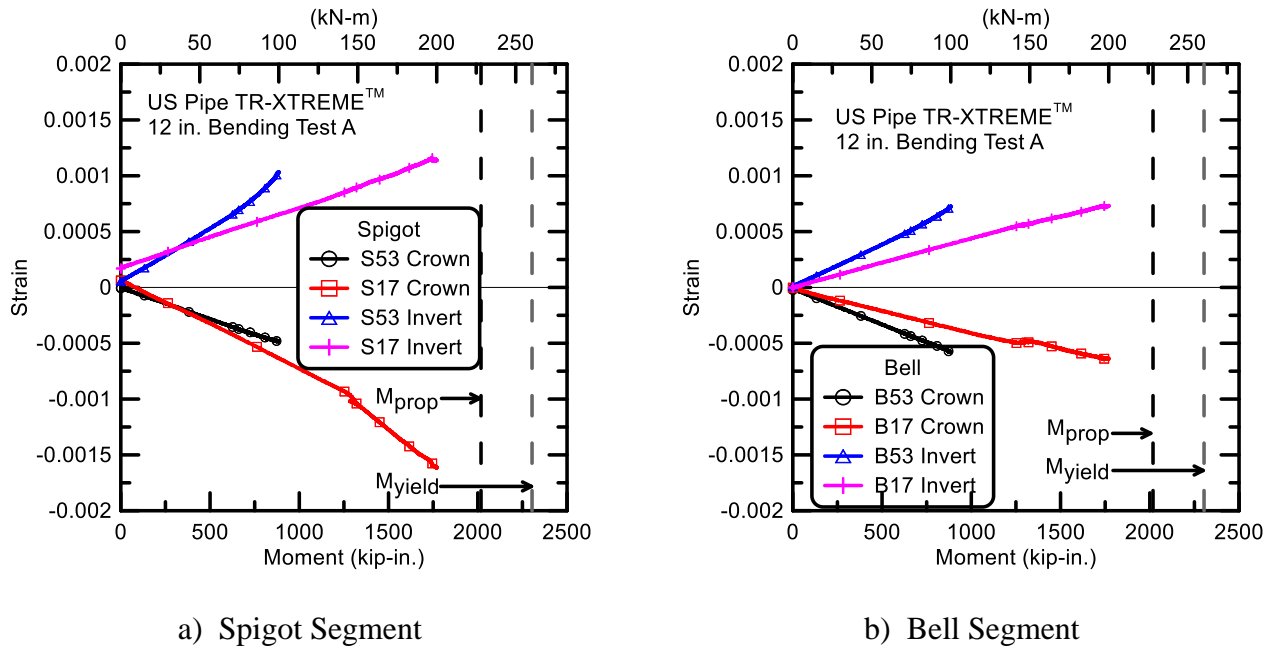


Figure 2.13. Strains on Spigot and Bell Segment vs. Applied Moment in Second Sequence of Test A

2.6 Test B Results

2.6.1 Pressure

Test B was pressurized with water to approximately 82 psi (565 kPa), and then the water transmitting line was turned off. Internal pressures fluctuated during bending, and the pressures were manually readjusted to maintain nearly constant pressure. Figure 2.14 shows the pressure vs. time data from Test B.

As shown in Figure 2.15 a), the first leakage (200 ml/min) was observed at 4.3 degrees of joint rotation, with a pressure drop to 43 psi (296 kPa). The water transmitting line was then turned on, and the remaining part of the test was run with internal pipe pressure of 80 psi (552 kPa). The rate of leakage slowly increased as the pipe continued to be loaded. A significant leakage of approximately 70 l/min was observed when the invert restraining clips slipped out of the joint. The test was then stopped. Figure 2.15 b) shows the final leakage of Test B.

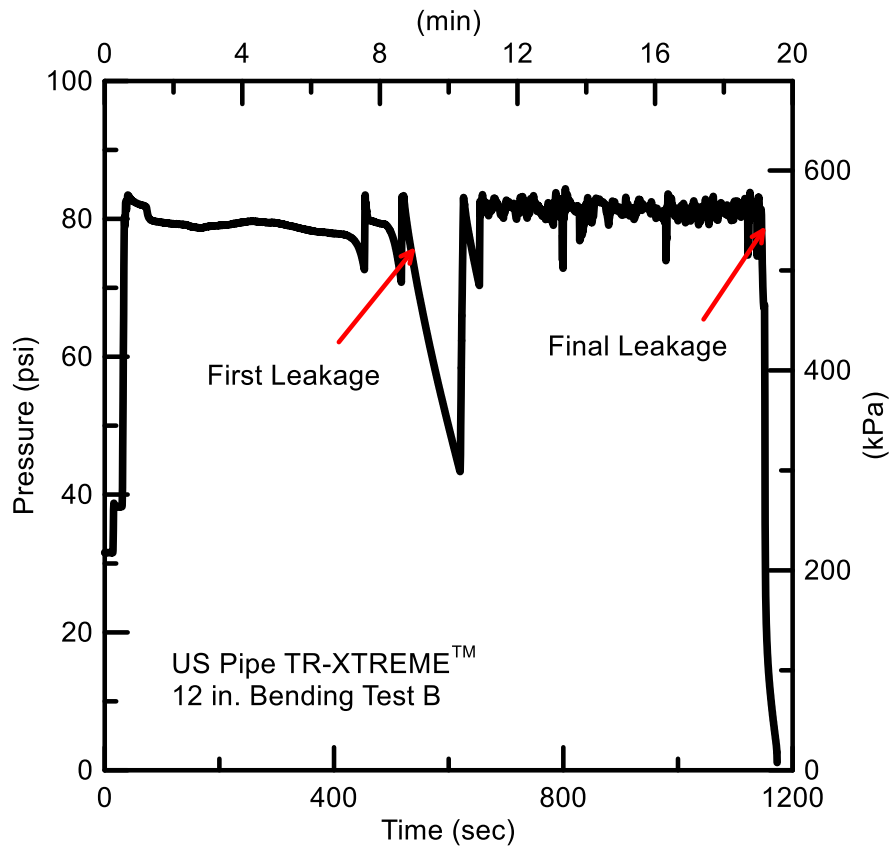


Figure 2.14. Pressure vs. Time for Test B



a) First Leakage



b) Final Leakage

Figure 2.15. Leakage of Test B

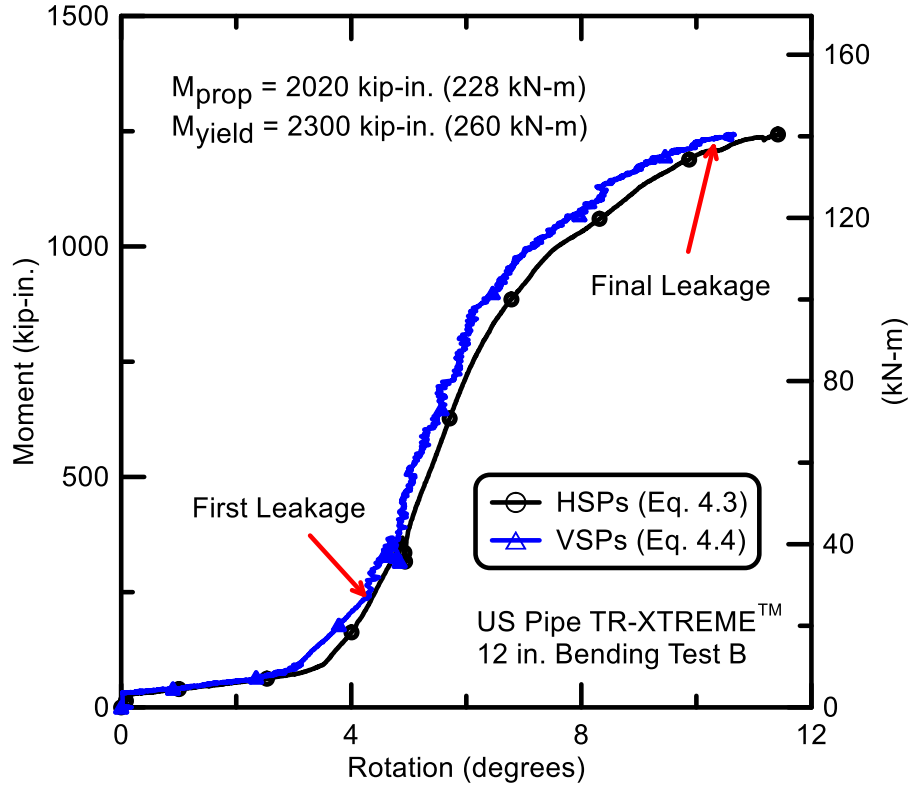


Figure 2.16. Moment-Rotation for Test B

2.6.2 Moment-Rotation

Joint rotations for Test B for the central portion of the bell and spigot joint were calculated using the horizontal string pots (HSPs) at the top and bottom of the bell (Eqn. 2.3) and using the three vertical string pots (VSPs) in the central portion (Eqn. 2.4). Figure 2.16 shows the moment-rotation data using both approaches. The moments are those imposed over the central pipe section. Only the rotations during the loading phase are shown. As shown in Figure 2.16, all measurement methods are in excellent agreement. The applied moments are well below the proportional limit of $M_{prop} = 2020$ kip-in (228 kN-m) [based on a proportional limit stress of $\sigma_{PL} = 39.5$ ksi (272 MPa)], and the yield limit, $M_y = 2300$ kip-in. (260 kN-m) [based on the yield stress of $\sigma_y = 45.1$ ksi (311 MPa)], as calculated from Equation 2.1.

First leakage was observed at an applied moment of 349 kip-in. (39.4 kN-m) and 4.8 degrees of joint rotation, which is the average rotation measured by the HSPs and VSPs (Eqns. 2.3 and 2.4).

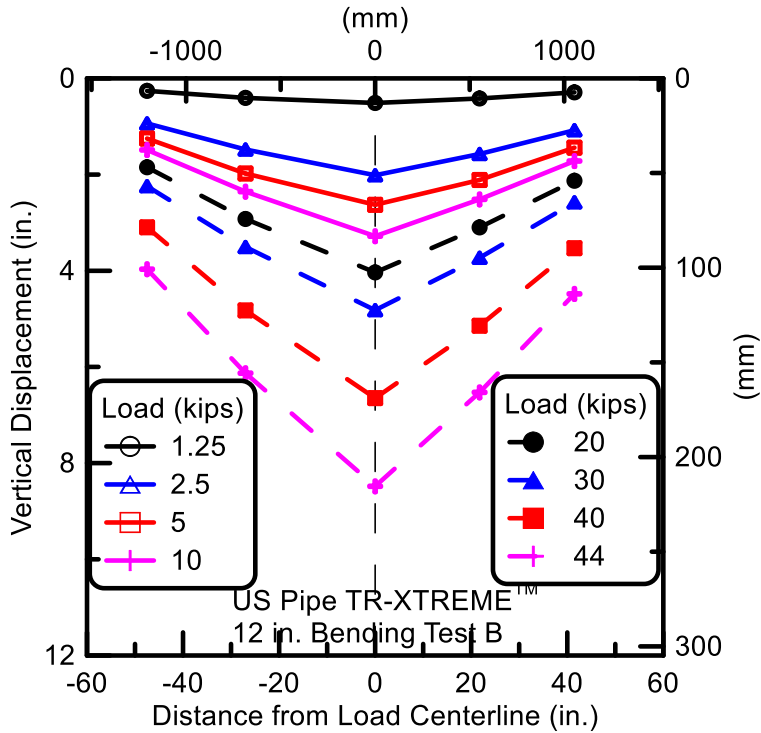


Figure 2.17. Vertical Displacements of Test B Specimen

The rate of leakage slowly increased as the pipe continued to be loaded. Final leakage of 70 l/min was observed at 1240 kip-in. (141 kN-m) and an average rotation of 11 degrees when the restraining clips at the invert slipped out of the joint.

2.6.3 Displacements

Pipe vertical displacements were measured at several distances along the pipe using VSPs. Figure 2.17 shows the VSP readings at these distances. In the figure positive displacements are downward, and positive distances from the load centerline are on the bell portion of the pipe. The displacements increased as the load increased, until significant leakage (approximately 70 l/min) was observed at 44 kips (196 kN). The pattern of displacements with load for Test B is nearly identical to that of Test A, but the vertical displacements of Test B are smaller than those of Test A.

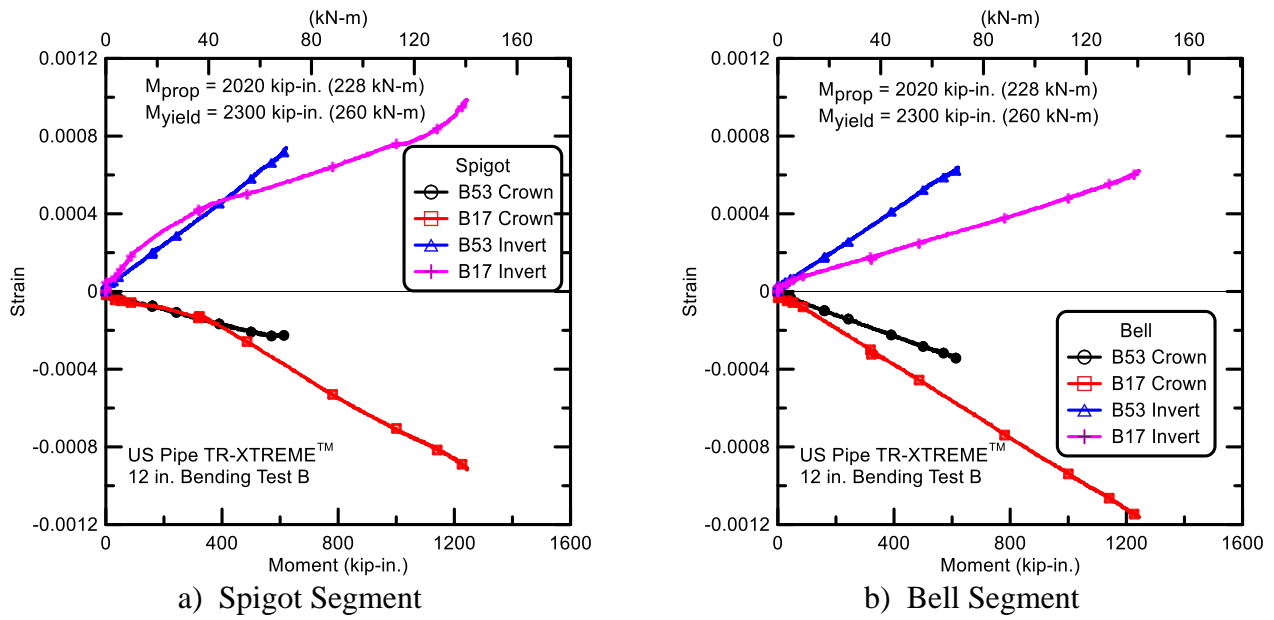


Figure 2.18. Strains on Spigot and Bell Segment vs. Applied Moment for Test B

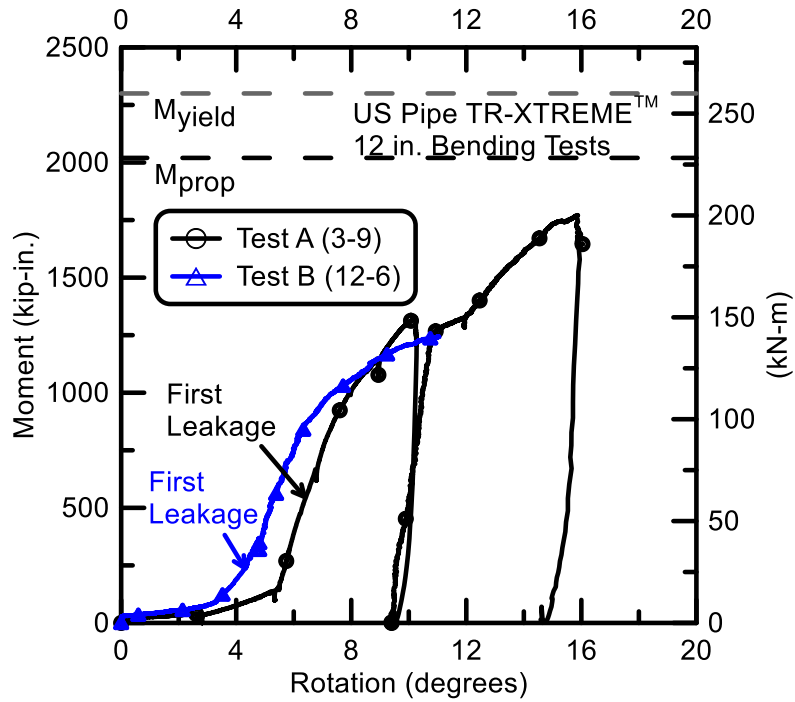


Figure 2.19. Moment – Rotations for Tests A and B

2.6.4 Pipe Strains

Figure 2.18 shows axial strains vs. applied moment for Test B. The strains decrease with distance from the pipe joint. Similar to Test A, the spigot strains at all gage planes are nearly the same for equal applied moments. Furthermore, the spigot strains are in reasonable agreement with the bell strains for the same applied moments.

2.7 Conclusions from Bending Tests

An important reason for performing Test A and Test B was to examine the differences in the moment vs. rotation relationship when the locking clips were at the 3 and 9 o'clock positions (Test A) and the 12 and 6 o'clock positions (Test B). Figure 2.19 shows the average rotations using the HSPs and VSPs for Tests A and B. First leakage was observed at a moment of 564 kip-in. (63.7 kN-m) and an average joint rotation of 6.5 degrees for Test A. The first leakage stopped after depressurization and did not occur again until a rotation of 10.3 degrees under 80 psi (552 kPa) internal pressure. The first leakage of Test B was detected at an applied moment of 350 kip-in. (39.4 kN-m) and 4.8 degrees of average joint rotation. The average rotation at first leakage for the two tests is 5.6 degrees.

The joints were able to sustain substantially higher moment and rotations beyond moment and rotation at first leakage. The maximum leakage of Test A occurred at an applied moment of 1770 kip-in. (200 kN-m) and an average joint rotation of 15.9 degrees. The test was terminated without significant damage or dislocation at the joint. The maximum leakage of Test B was observed at an applied moment of 1240 kip-in. (141 kN-m) and an average joint rotation of 11 degrees. The test was terminated when the invert restraining clips slipped out of the joint.

The moment vs. rotation relationships for the two tests are similar up to a rotation of approximately 10 degrees. Higher moments were mobilized at smaller rotation angles when the clips were positioned closer to the 12 and 6 o'clock positions in alignment with the applied load. The maximum moments developed in both tests were well below both the proportional limit moment, M_{prop} , and the yield moment, M_{yield} .

Section 3

Joint Tension Test

3.1 Introduction

This report section summarizes the results of the tension testing of the US Pipe TR-XTREME™ joint. Two tension tests were conducted.

3.2 Tension Test 1

The pipe joint specimen was 160-in. (4.56 m)-long and 0.415-in. (10.5 mm)-thick with the outside diameter of 13.13 in. (334 mm). The pipe was placed in the load frame so that its restraining clips were located near the 12 and 6 o'clock (crown and invert) positions. The pipe was initially fully inserted in the bell at the beginning of the test. Fully inserted refers to the position when either the weld bead was in contact with the bell throat, or the end of the spigot was in contact with the base of the bell socket. A schematic of the tension test is provided in Figure 3.1.

3.2.1 Instrumentation

Four strain gages were mounted 36 in. (914 mm) north of the bell face on the bell side of the pipe at the positions of 12, 3, 6, and 9 o'clock (crown, east, invert, and west, respectively). The other four strain gages were mounted 33.5 in. (851 mm) south of the bell face on the spigot side at the same positions. Four string pots, mounted to the spigot at quarter points around the pipe circumference 16 in. (406 mm) from the bell face, were fixed to the bell and used to measure axial pullout of the spigot from the bell. An actuator and twelve load cells were installed on the load frame to apply and measure tensile force at the end of the pipe. The instrument locations and gage names are listed in Table 3.1.

3.2.2 Force – Displacement

The pipe was filled with water and pressurized. The pressurizing sequence is shown in Figure 3.2. As the pressure was increased to 6.27 psi (43.2 kPa), there was a very small pullout movement of the spigot, after which there was a sudden displacement to 2.43 in. (61.7 mm). The pressure was then raised to the target of 80 psi (552 kPa) in preparation for axial loading.

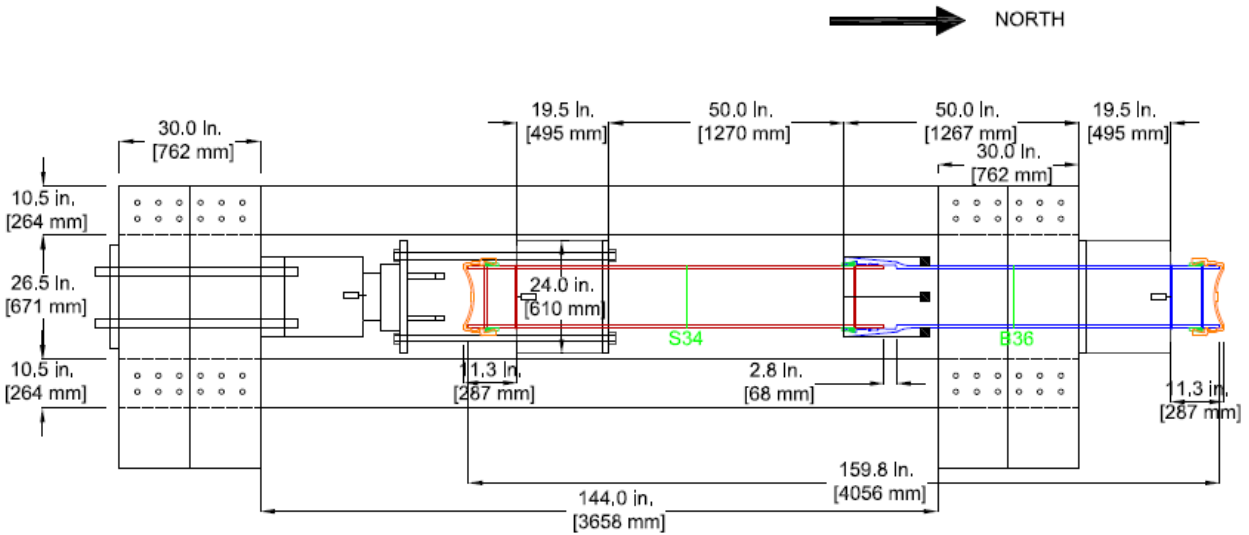


Figure 3.1. Tension Test Layout

Table 3.1. Instrumentation for US Pipe TR-XTREME™ Joint Tension Test 1

Location	Instrument	Local Instrument Name
36 in. North of Bell Face	Crown, Axial Strain	B36C
36 in. North of Bell Face	Invert, Axial Strain	B36I
36 in. North of Bell Face	East Springline, Axial Strain	B36E
36 in. North of Bell Face	West Springline, Axial Strain	B36W
33.5 in South of Bell Face	Crown, Axial Strain	S34C
33.5 in South of Bell Face	Invert, Axial Strain	S34I
33.5 in South of Bell Face	East Springline, Axial Strain	S34E
33.5 in South of Bell Face	West Springline, Axial Strain	S34W
Bell Face	Crown String Pot	Jnt Opening C
Bell Face	Invert String Pot	Jnt Opening I
Bell Face	East Springline String Pot	Jnt Opening E
Bell Face	West Springline String Pot	Jnt Opening W
Actuator	Load Cell	LC1
Actuator	Load Cell	LC2
Actuator	Load Cell	LC3
Actuator	Load Cell	LC4
Actuator	Load Cell	LC5
Actuator	Load Cell	LC6
Actuator	Load Cell	LC7

Table 3.1. Instrumentation for US Pipe TR-XTREME™ Joint Tension Test 1 (completed)

Location	Instrument	Local Instrument Name
Actuator	Load Cell	LC8
Actuator	Load Cell	LC9
Actuator	Load Cell	LC10
Actuator	Load Cell	LC11
Actuator	Load Cell	LC12
Actuator	Displacement	Act Disp

1 in. = 25.4 mm

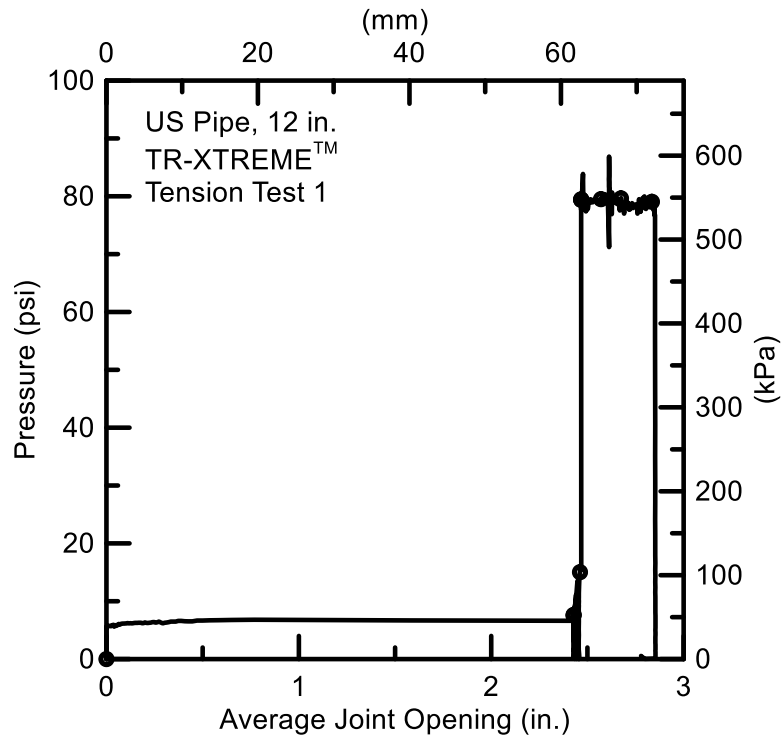


Figure 3.2. Pressure vs. Average Joint Opening of Tension Test 1

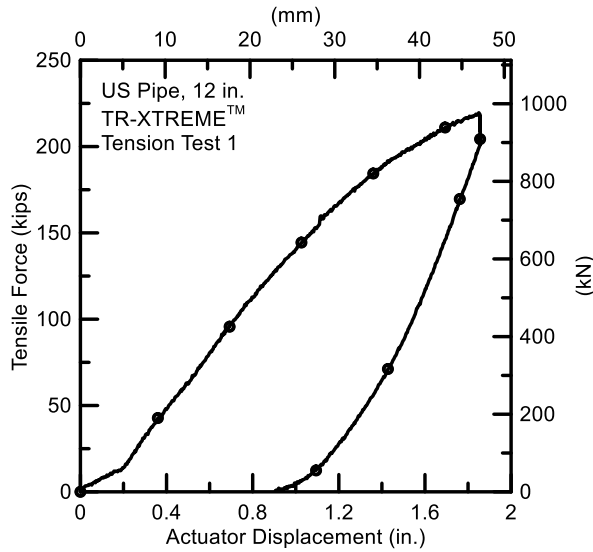


Figure 3.3. Tensile Force vs. Actuator Displacement of Test 1

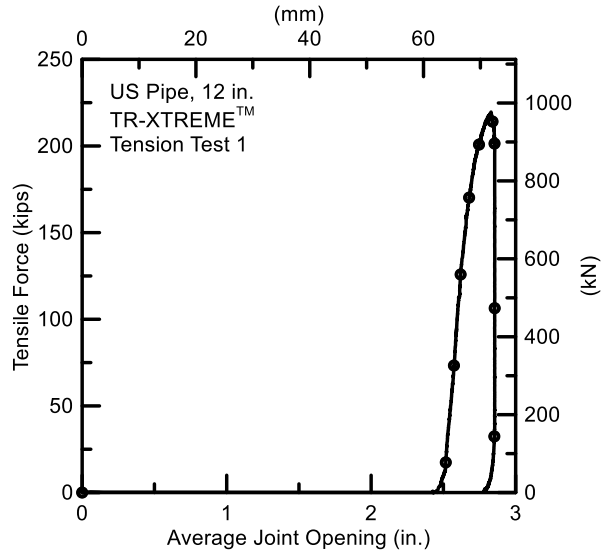


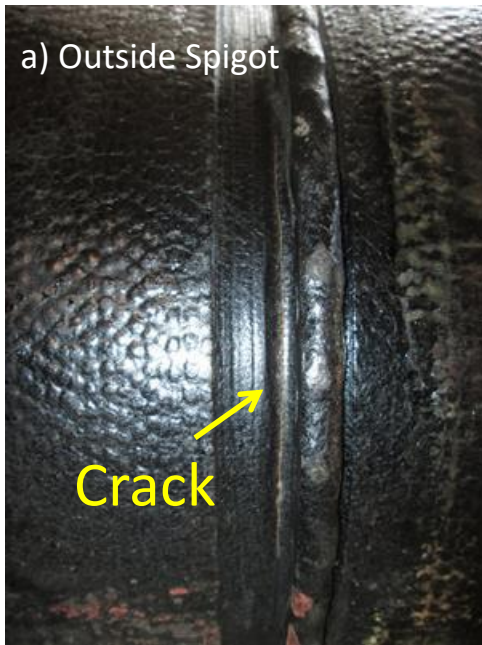
Figure 3.4. Tensile Force vs. Average Joint Opening of Test 1

During the pressurizing phase, the load cells were damaged and did not function properly for the remaining part of the test. Therefore, the load applied in this test was calculated using the strains on the bell and spigot segments. The load, P , is given by Equation 3.1, as follows

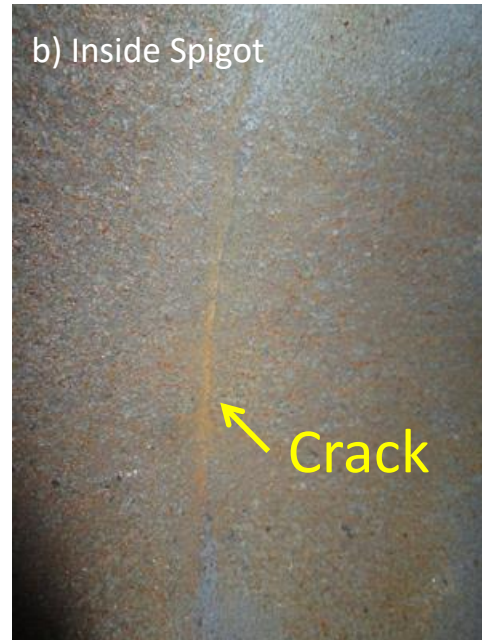
$$P = \varepsilon EA \quad (3.1)$$

where ε is the measured strain on each segment of the specimen, and E is Young's modulus of ductile iron of 27,000 ksi (186 GPa) based on the tensile test data from commercially available ductile iron pipe reported by Wham and O'Rourke (2015). The cross-sectional area, A , of the specimen was 16.6 in² (107 cm²).

The pipe was secured to the actuator, and loading began at a rate of 0.2 in. (5.1 mm) per minute. Figures 3.3 and 3.4 show the tensile force plotted against actuator displacement and average joint opening, respectively. A peak load of 219.6 kips (977 kN), which was calculated from the average of all eight strain gages on both the bell and spigot, was attained at 1.85 in. (47 mm) of actuator displacement and 2.83 in. (71.9 mm) of joint opening. The load then decreased slightly as a circumferential crack appeared at the east springline of the spigot behind the weld bead. Figure 3.5 shows photos of the crack on the inside and outside of the spigot. The crack caused the first leakage (200 ml/min) at 216 kips (960 kN) of tensile force with 1.86 in. (47.2 mm) and 2.84 in. (72.1 mm) of actuator displacement and joint opening, respectively. Figure 3.6 a) shows



a) Outside Spigot



b) Inside Spigot

Figure 3.5. Circumferential Crack on East Springline of Spigot of Test 1

the first leakage of the test. The leakage reached the maximum rate of about 10 liters per minute, as shown in Figure 3.6 b), at 1.86 in. (47.2 mm) of actuator displacement and 2.85 in. (72.4 mm) of joint opening. The calculated load at the maximum leakage was 211 kips (939 kN).

3.2.3 Spigot Deformations

The diameter of the spigot was measured at four different locations: Crown to Invert (C to I), Crown East to Invert West (CE to IW), East to West (E to W) and Invert East to Crown West (IE to CW) as shown in Figure 3.7. The outer diameter of the spigot was measured before the tension test. The measurements showed that the spigot had a circular cross-section with a 13.13 in. (334 mm) diameter along its length.

As tensile force was applied, the spigot was pulled from the bell, thus causing the weld bead on the spigot to bear against the restraining clips. As the tensile force increased, the load that the restraining clips carried also increased.



a) First Leakage



b) Maximum Leakage

Figure 3.6. Leakage of Test 1

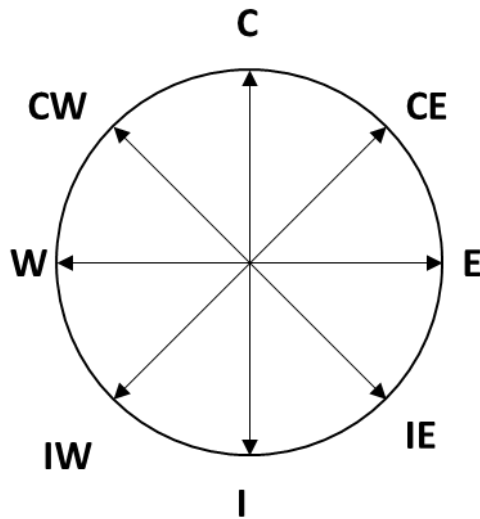


Figure 3.7. Spigot Measurement Locations (Looking North)

Table 3.2. Diameter Measurements on Spigot Section for Test 1

Pre-Test				
Locations	C-I (in.)	CE-IW (in.)	E-W (in.)	CW-IE (in.)
Spigot End	13.132	13.130	13.131	13.128
Post-Test				
Locations	C-I (in.)	CE-IW (in.)	E-W (in.)	CW-IE (in.)
3 in. from End	13.173	13.150	13.181	13.150
4 in. from End	13.185	13.150	13.228	13.150
7.25 in. from End	13.130	13.055	13.268	13.071
8 in. from End	13.169	13.150	13.260	13.146
42 in. from End	13.138	13.138	13.130	13.118

Diameter measurements after the test were taken at 5 different locations along the length of the spigot at 3 in. (76.2 mm), 4 in. (102 mm), 7.25 in. (184 mm) (clips bearing areas), 8 in. (203 mm), and 42 in. (1067 mm) away from the end of the spigot (strain gage location), as shown in Figures 3.8 (a), (b), and (c). The diameter measurements are presented in Table 3.2.

The E-W diameter measurements are slightly larger than the C-I, CE-IW, and CW-IE diameter measurements, with the E-W diameter between 0.03 and 0.13 in. (0.76 mm and 3.30 mm) larger within 8 in. (200 mm) from the end of the spigot. Recall that the restraining clips were located near crown and invert positions. Thus, the spigot would tend to flatten and extend along the E-W diameter as it was pulled through the clips. Figure 3.9 is a photo of the area where the restraining clips transferred the load onto the spigot.

3.2.4 Spigot Axial Strains

The maximum tensile axial strain on the spigot side was $782 \mu\epsilon$ (0.0782%) and developed at the crown under an average spigot load (Eqn. 3.1) of 217 kips (966 kN) at 1.86 in. (47.2 mm) of actuator displacement and 2.83 inches (71.9 mm) of joint opening. The crown axial strain was $777 \mu\epsilon$ (0.0777%) at first leakage and $768 \mu\epsilon$ (0.0768%) at maximum leakage. The relationships between spigot axial strains and both the tensile force and joint opening are shown in Figures 3.10 and 3.11, respectively. Recall that there was a rapid joint opening of roughly 2.43 in. (61.7 mm) as internal pressure was applied.



a) On Spigot Section



b) Close to Spigot End



c) 42 in. from Spigot End

Figure 3.8. Diameter Measurement Locations on Spigot Section



Figure 3.9. Restraining Clips Bearing Area on the Spigot of Test 1

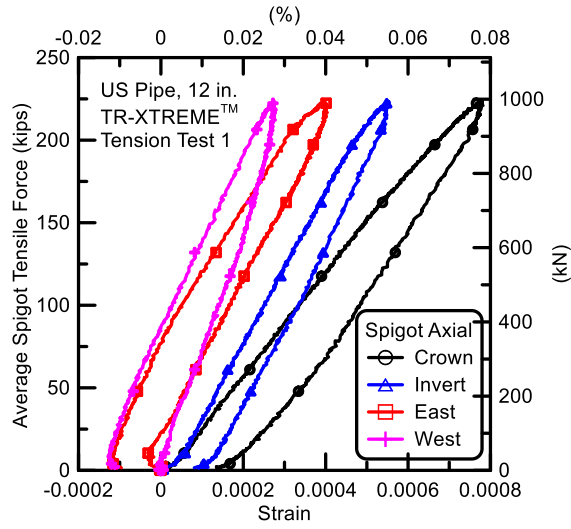


Figure 3.10. Average Spigot Tensile Force vs. Spigot Axial Strain of Test 1

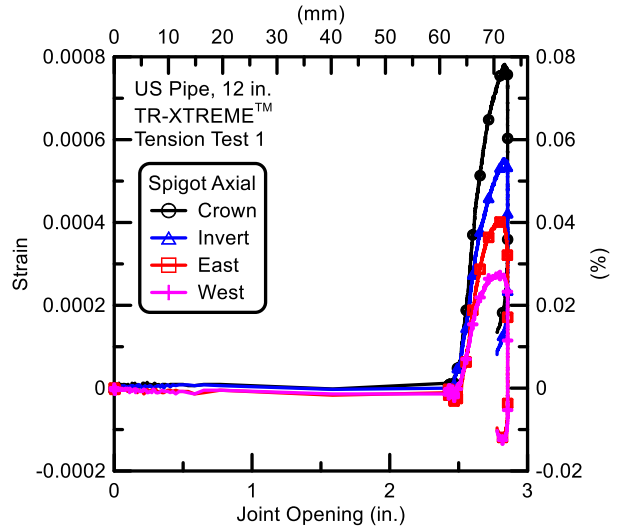


Figure 3.11. Spigot Axial Strain vs. Average Joint Opening of Test 1

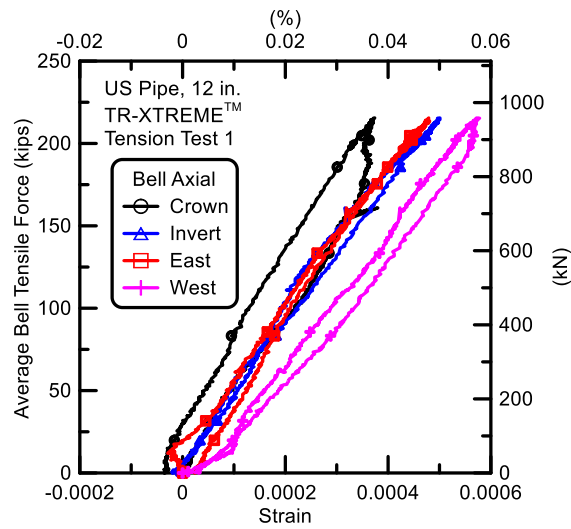


Figure 3.12. Average Bell Tensile Force vs. Spigot Axial Strain of Test 1

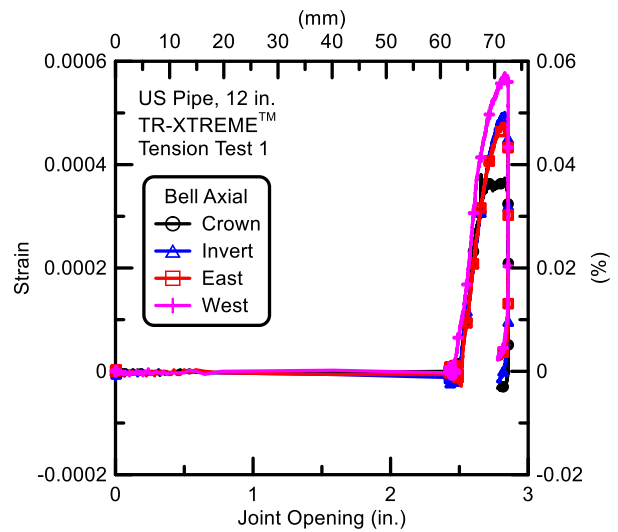


Figure 3.13. Bell Axial Strain vs. Average Joint Opening of Test 1

3.2.5 Bell Axial Strains

The actuator tensile force vs. axial bell strain and axial bell strain vs. actuator displacement are shown in Figures 3.12 and 3.13, respectively. The maximum tensile axial strain measured in the bell was $578 \mu\epsilon$ (0.0578%) on the west side. The average bell load was 219 kips (974 kN) (Eqn. 3.1), with a corresponding actuator displacement and joint opening of 1.85 in. (47.0 mm) and 2.83 in. (71.9 mm), respectively. The west axial strain was $572 \mu\epsilon$ (0.0572%) at the first leakage and $569 \mu\epsilon$ (0.0569%) at the maximum leakage.

3.3 Tension Test 2

A second tension test was performed on a prototype US Pipe TR-XTREME™ joint. The purpose of this test was to provide a replicate test to confirm joint behavior and monitor more closely the restraining clip movements at the joint. The pipe was set in the load frame so that its restraining clips were at the 3 and 9 o'clock (east and west) positions. The pipe was initially fully inserted in the bell. The pipe dimensions were identical to that of Test 1.

3.3.1 Instrumentation

The instrumentation of Test 2 was similar to that of Test 1. However, the twelve load cells used in Test 1 (see Table 3.1) were removed and replaced with ALD-300K load cell. The instrument locations and local gage names of Test 2 are listed in Table 3.3.

3.3.2 Force – Displacement

The pipe was filled with water and pressurized. The pressurizing sequence is shown in Figure 3.14. As the pressure was increased to 6 psi (41 kPa), there was a very small pullout movement of the spigot, after which there was a sudden displacement to 2.27 in. (57.7 mm). The pressure was then raised to the target of 82 psi (565 kPa) in preparation for axial loading.

The pipe was secured to the actuator, and loading began at a rate of 0.4 in. (10.2 mm) per minute. Figures 3.15 and 3.16 show the tensile force plotted against actuator displacement and average joint opening, respectively. A peak load of 259 kips (1150 kN) was attained at 1.32 in. (33.5 mm) of actuator displacement and 2.92 in. (74.2 mm) of joint opening. The load then decreased until the spigot was dislodged abruptly from the bell, causing a large amount of leakage, as shown in Figure 3.17. The measured load at failure was 257 kips (1140 kN) at 1.39 in. (35.3 mm) of actuator displacement and 2.99 in. (75.9 mm) of joint opening.

Table 3.3. Instrumentation for US Pipe TR-XTREME™ Joint Tension Test 2

Location	Instrument	Local Instrument Name
36 in. North of Bell Face	Crown, Axial Strain	B36C
36 in. North of Bell Face	Invert, Axial Strain	B36I
36 in. North of Bell Face	East Springline, Axial Strain	B36E
36 in. North of Bell Face	West Springline, Axial Strain	B36W
33.5 in South of Bell Face	Crown, Axial Strain	S34C
33.5 in South of Bell Face	Invert, Axial Strain	S34I
33.5 in South of Bell Face	East Springline, Axial Strain	S34E
33.5 in South of Bell Face	West Springline, Axial Strain	S34W
Bell Face	Crown String Pot	Jnt Opening C
Bell Face	Invert String Pot	Jnt Opening I
Bell Face	East Springline String Pot	Jnt Opening E
Bell Face	West Springline String Pot	Jnt Opening W
Actuator	Load Cell	ALD-300K Load Cell
Actuator	Displacement	Act Disp

1 in. = 25.4 mm

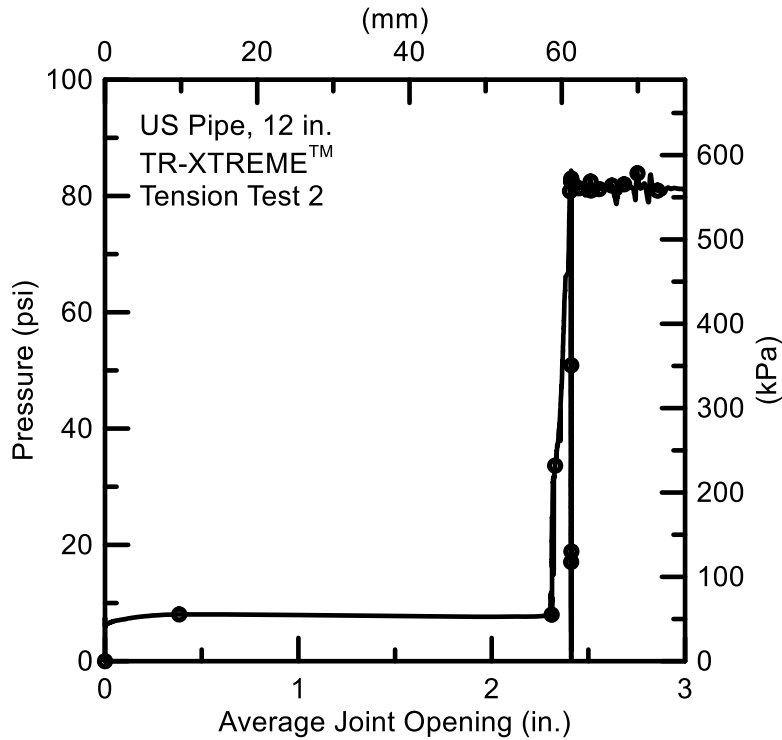


Figure 3.14. Pressure vs. Average Joint Opening of Test 2

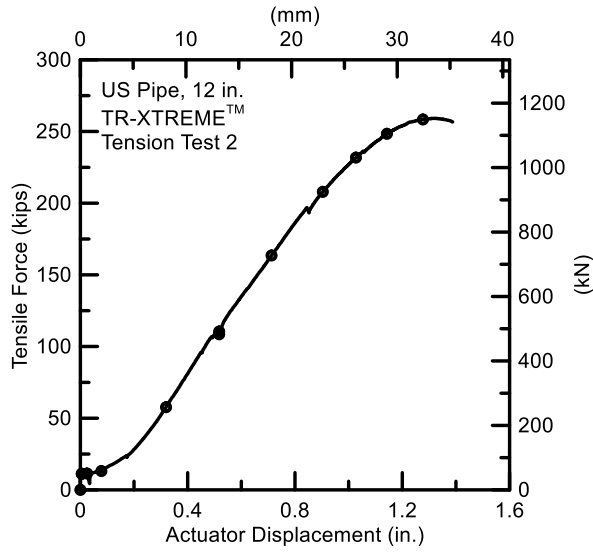


Figure 3.15. Tensile Force vs. Actuator Displacement of Test 2

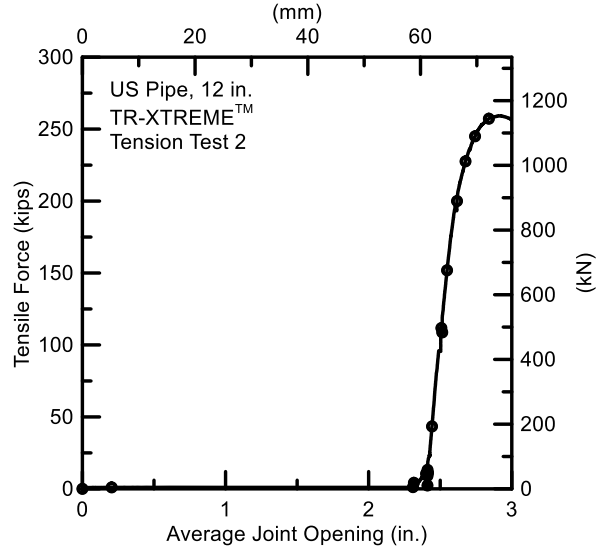


Figure 3.16. Tensile Force vs. Average Joint Opening of Test 2

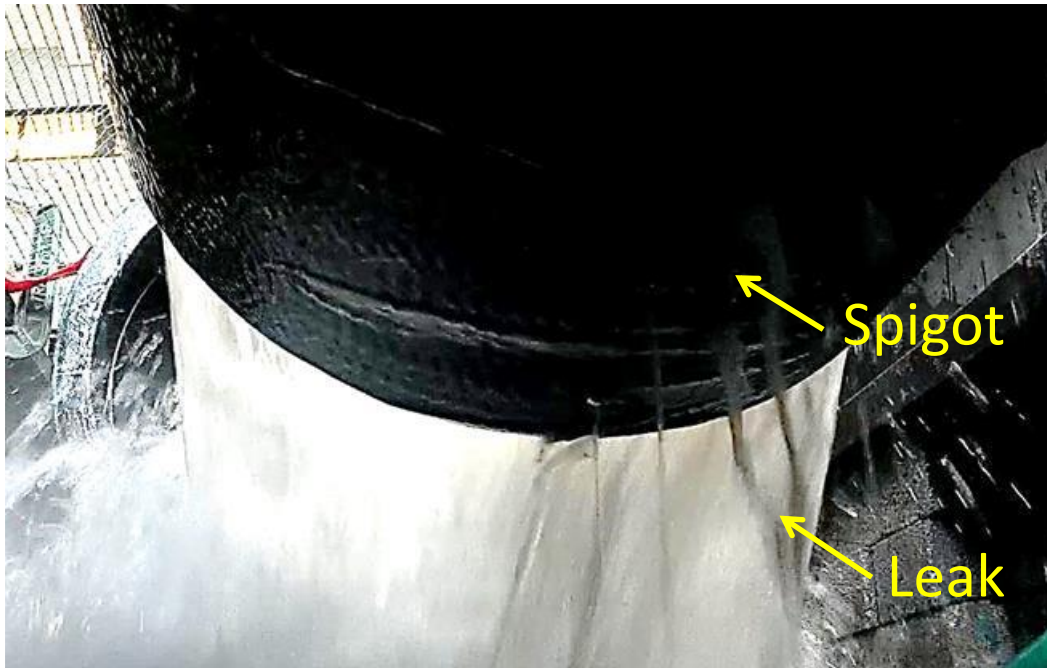


Figure 3.17. Leakage at Failure of Test 2 (Looking Invert)

Table 3.4. Diameter Measurements on Spigot Section for Test 2

Pre-Test				
Locations	C-I (in.)	CE-IW (in.)	E-W (in.)	CW-IE (in.)
Spigot End	13.130	13.129	13.130	13.128
Post-Test				
Locations	C-I (in.)	CE-IW (in.)	E-W (in.)	CW-IE (in.)
3 in. from End	13.169	13.150	13.091	13.051
4 in. from End	13.189	13.150	13.071	13.071
7.25 in. from End	13.346	13.032	13.051	12.972
8 in. from End	13.327	13.051	13.091	13.051
42 in. from End	13.130	13.071	13.130	13.189

The pipe had a large circumferential crack on the bell section. Figure 3.18 shows the Test 2 specimen at pipe rupture. Figure 3.18 a) is a view looking into the bell. Figures 3.18 b) to d) show the bell crack starting at the crown [Figure 3.18 b) and rotating clockwise to the invert [Figure 3.18 d)]. Figures 3.18 f) and g) show views of the fracture from inside the bell.

3.3.3 Spigot Deformations

Similar to Test 1, the diameter of the spigot was measured at four different locations: Crown to Invert (C to I), Crown East to Invert West (CE to IW), East to West (E to W) and Invert East to Crown West (IE to CW) as shown in Figure 3.7. The outer diameter of the spigot was measured before the tension test. The measurements showed that the spigot had an identical circular cross-section to that of Test 1 with a 13.13 in. (334 mm) diameter along its length.

Diameter measurements after the test were taken at 5 different locations along the length of the spigot similar to Test 1. The diameter measurements are presented in Table 3.4. The C-I diameter measurements are slightly larger than the E-W, CE-IW, and CW-IE diameter measurements, with the C-I diameter between 0.02 and 0.38 in. (0.51 mm and 9.65 mm) larger within 8 in. (200 mm) from the end of the spigot. Recall that the restraining clips were located near east and west springlines. Thus, the spigot would tend to flatten and extend along the C-I



a) Bell Face



b) Crown



c) East Springline



d) Invert



f) Inside East Springline



g) Inside Crown

Figure 3.18. Circumferential Crack on Bell Section in Test 2



Figure 3.19. Restraining Clips Bearing Area on the Spigot of Test 2

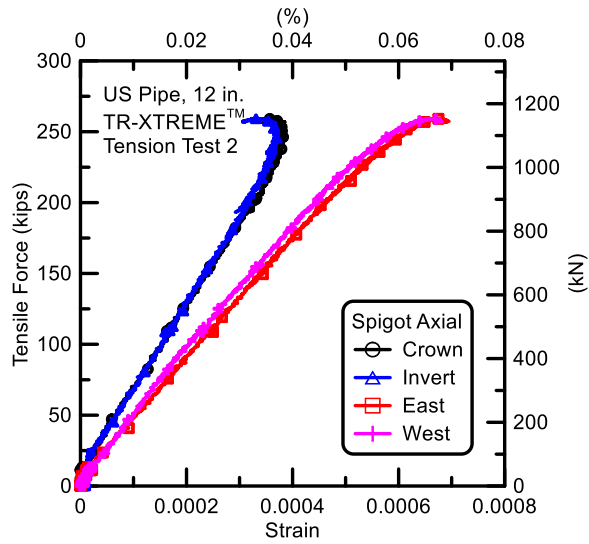


Figure 3.20. Tensile Force vs. Spigot Axial Strain of Test 2

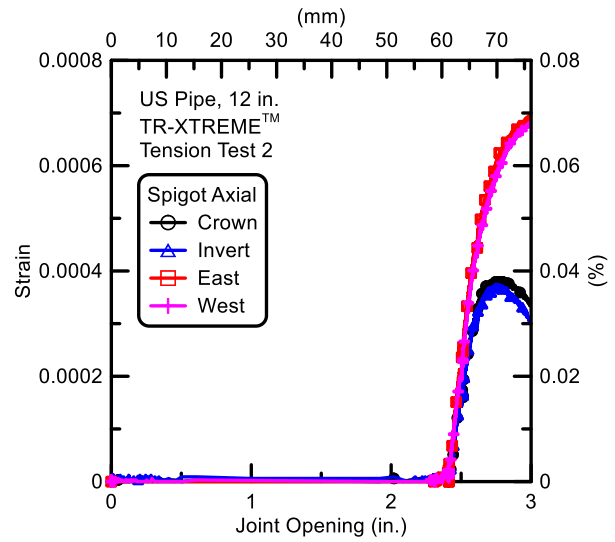


Figure 3.21. Spigot Axial Strain vs. Average Joint Opening of Test 2

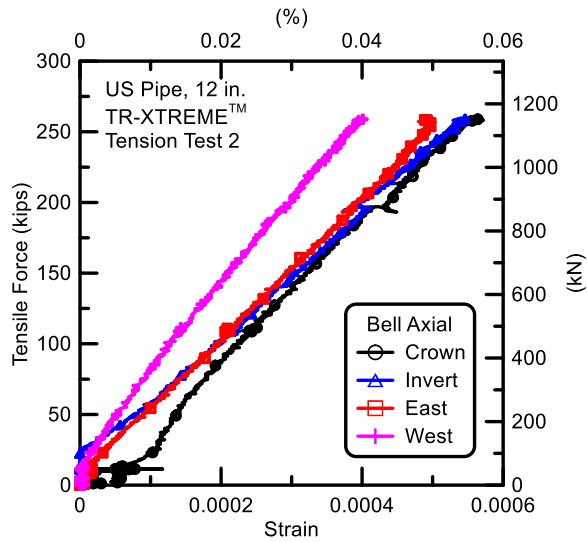


Figure 3.22. Tensile Force vs. Bell Axial Strain of Test 2

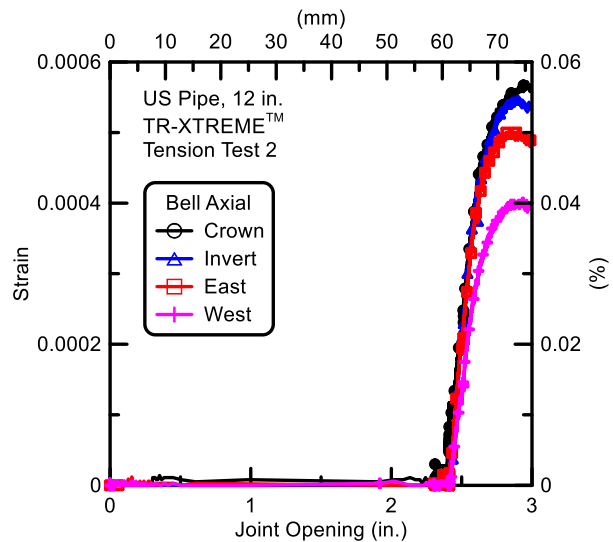


Figure 3.23. Bell Axial Strain vs. Average Joint Opening of Test 2

diameter as it was pulled through the clips. Figure 3.19 is a photo of the area where the restraining clips transferred the load onto the spigot

3.3.4 Spigot Axial Strains

The maximum tensile axial strain on the spigot side was $695 \mu\epsilon$ (0.0695%) and developed at the east springline under an applied load of 257 kips (1145 kN) at 1.38 in. (35.1 mm) of actuator displacement and 2.98 inches (75.7 mm) of average joint opening. The east axial strain was $689 \mu\epsilon$ (0.0689%) at failure. The relationships between spigot axial strains and both the tensile force and joint opening are shown in Figures 3.20 and 3.21, respectively. Recall that there was a rapid joint opening of roughly 2.27 in. (57.7 mm) as internal pressure was applied. The axial strains in the spigot were nearly zero as the spigot moved out of the bell under internal pressure.

3.3.5 Bell Axial Strains

The actuator tensile force vs. axial bell strain and axial bell strain vs. actuator displacement are shown in Figures 3.22 and 3.23, respectively. The maximum tensile axial strain measured in the bell was $572 \mu\epsilon$ (0.0572%) at the crown. The axial load was 258 kips (1150 kN), with a corresponding actuator displacement and joint opening of 1.36 in. (34.5 mm) and 2.96 in. (75.2 mm), respectively. The crown axial strain was $567 \mu\epsilon$ (0.0567%) at failure.

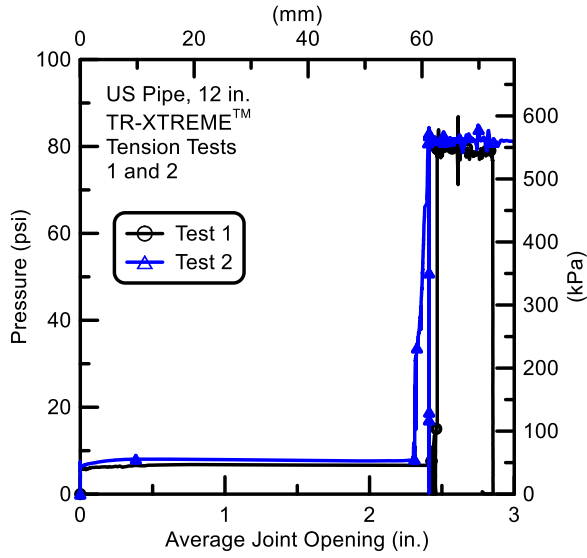


Figure 3.24. Pressure vs. Average Joint Opening for Tests 1 and 2

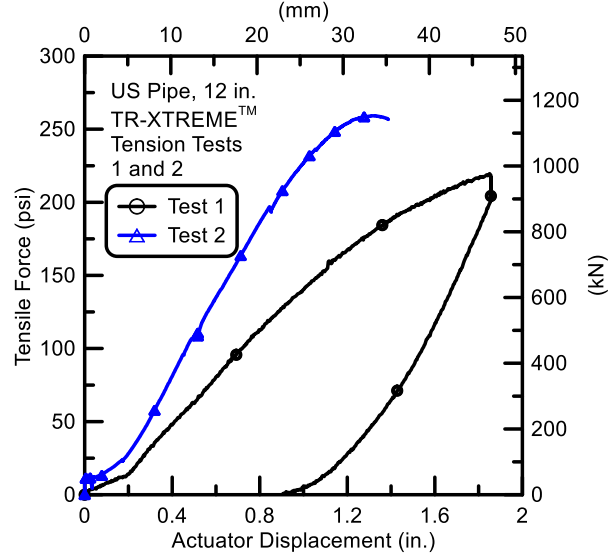


Figure 3.25. Tensile Force vs. Actuator Displacement for Tests 1 and 2

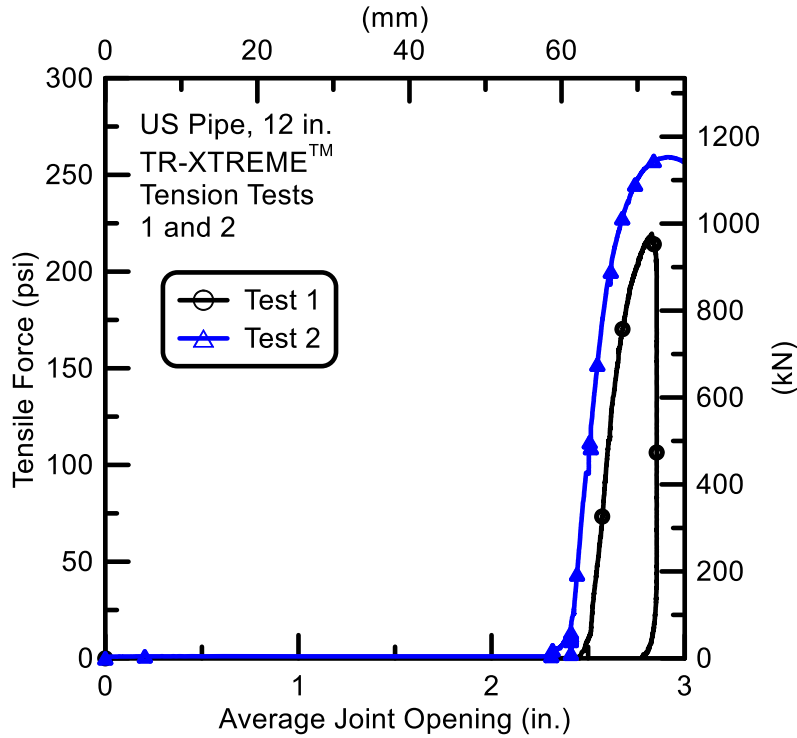


Figure 3.26. Tensile Force vs. Average Joint Opening for Tests 1 and 2

3.4 Tests 1 and 2 Comparisons

This section presents a comparison of the two test results. Figure 3.24 shows that a continuous internal pressure of 80-82 psi (552-565 kPa) was maintained for both tests. As shown in Figure 3.25, Tests 1 and 2 reached a maximum axial force of 220 kips (977 kN) and 259 kips (1150 kN), respectively.

Figure 3.26 shows tensile force vs. average joint opening for the two tests. An initial axial slip of 2.43 in. (61.7 mm) and 2.27 in. (57.7 mm) in Test 1 and 2, respectively, was measured as the spigot was pulled from the bell until the weld bead on the spigot was bearing against the restraining clips. After the weld bead made contact with the clips, an additional 0.4 in. and 0.7 in. (10 mm and 18 mm) of axial displacement was measured in Test 1 and 2, respectively, before cracking was observed. Tests 1 and 2 reached a maximum joint opening of 2.83 in. (71.9 mm) and 2.92 in. (74.2 mm) at a maximum axial load of 220 kips (977 kN) and 259 kips (1150 kN), respectively.

Test 1 was accompanied by some eccentric loading that was not developed in Test 2. The lower maximum axial force in Test 1 reflects the load eccentricity. The maximum axial load of 259 kips (1150 kN) in Test 2 is more representative of the axial load capacity of the 12-in (304.8-mm)-diameter joint.

3.5 Conclusions

Two tension tests were performed on the 12-in. (300-mm)- diameter US Pipe TR- XTREME™ joint. Both tests began with the spigot fully inserted in the bell. As the pipe was pressurized, the spigot was displaced from the bell seat at approximately 6 psi internal pressure. The slip was 2.43 in. (61.7 mm) and 2.27 in. (57.7 mm) before the weld bead became engaged with the restraining clips for Tests 1 and 2, respectively. Tests 1 and 2 reached a maximum force of 220 kips (977 kN) at 2.83 in. (71.9 mm) of axial displacement and a maximum axial load of 259 kips (1150 kN) at 2.92 in. (74.2 mm) of joint displacement, respectively. The onset of leakage is caused by forces generated between the spigot bead and restraining clips that crack the bell circumferentially. The joints began to leak at openings of 2.84 and 2.99 in. (72.1 mm and 75.9 mm) for Tests 1 and 2, respectively. After the weld bead on the spigot made contact with the clips, an additional movement between 0.4 and 0.7 in. (10 mm and 18 mm) was required to generate leakage at the joint.

The maximum axial load of 259 kips (1150 kN) in Test 2 is more representative of the axial load capacity of the 12-in. (300-mm)- diameter US Pipe TR- XTREME™ joint and should be used as a best estimate of maximum load capacity for direct axial loading. The maximum axial load caused cracking of the pipe bell. The maximum axial load occurred at a displacement of 2.92 in. (74.2 mm). Given an initial slip of 2.27 in. (57.7 mm) to engage contact between the spigot bead and restraining clips, an additional movement of approximately 0.65 in. (17 mm) was required to initiate cracking of the bell and leakage at the joint.

Section 4

Finite Element Simulations

Two-dimensional (2D) finite element (FE) analyses were performed for 4-, 6-, 8-, 12-, 14-, and 16- in. (100-, 150-, 200-, 300-, 350-, and 400-mm, respectively)-diameter DI pipelines using soil and geometric parameters consistent with the large-scale test basin experiment presented in a previous report for US Pipe (Cornell University, 2015). The purpose of these analyses is to demonstrate the performance of DI pipelines with TR-XTREME™ pipe joints, based on numerical simulation, to the same ground deformation imposed on the 6-in. (150-mm) pipeline in the previous large-scale split-basin test.

4.1 Large-Scale Split Basin Test

Figure 4.1 is a plan view of the large-scale split basin test layout, which was used to generate fault rupture effects of 6-in. (150-mm)- diameter DI pipeline consisting of five pipe segments connected with TR-XTREME™ joints. The figure shows the fault rupture plane and approximate locations of the four actuators driving the ground failure. A detailed description of the test is provided by Cornell University (2015), and only the salient features of the testing are summarized in this report.

The objective of the test was to impose abrupt ground deformation on the pipeline, which was identical to left lateral strike slip fault rupture and representative of the most severe ground deformation that occurs along the margins of liquefaction-induced lateral spreads and landslides. The pipeline was constructed to evaluate its capacity to accommodate full-scale fault movement through the simultaneous axial pullout at four different joints. Measuring simultaneous performance of multiple joints allows for confirmation that the pipeline will respond to ground failure as intended, understand the complex interaction among the different joints, and determine the maximum ground deformation and axial pipeline load that can be sustained before joint leakage.

The pipeline was buried in the Cornell large-scale test basin in partially saturated sand that was compacted to have an average friction angle of 42°, equivalent in strength to that of a medium dense to dense granular backfill. The pipeline was laid out so that the spigot at each joint could pull from the bell approximately 2.3 in. (58 mm) before the spigot bead made contact with the

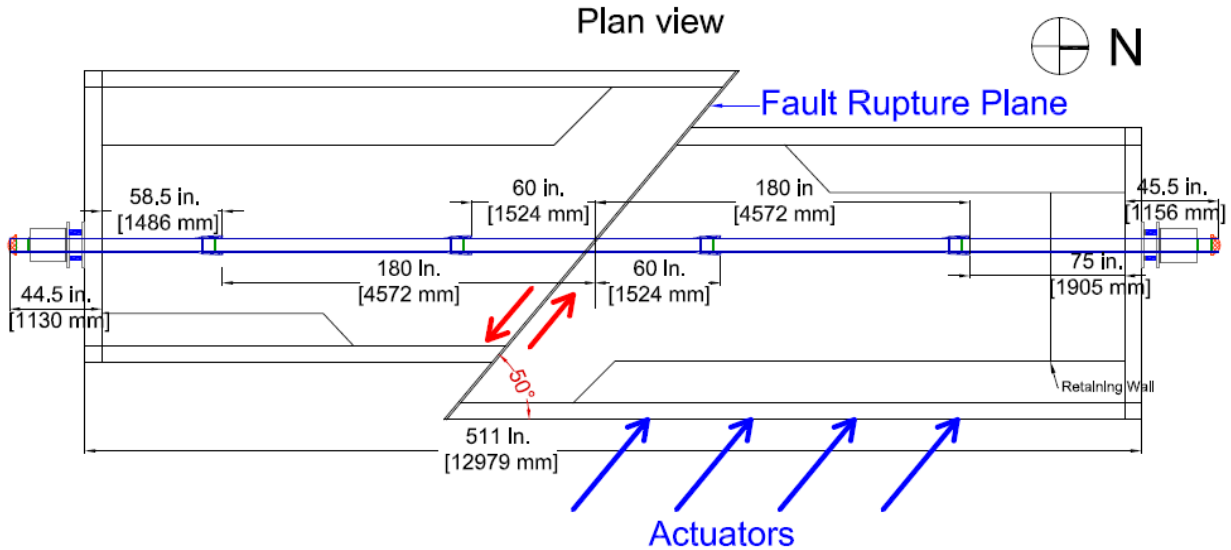


Figure 4.1. Plan View of Large-Scale Split Basin Test

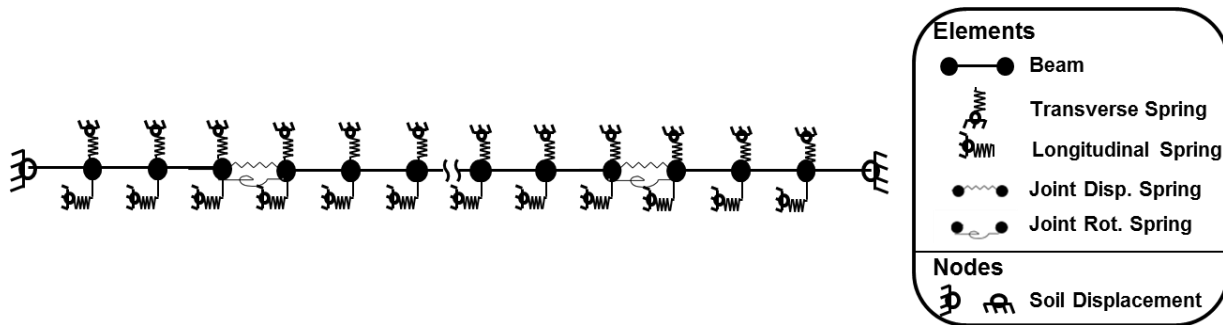


Figure 4.2. 2D FE Model Setup for a Pipeline under Fault Rupture

restraining clips. Approximately 0.5 in. (13 mm) was available for compression at each joint. The depth of burial to top of pipe was 2.5 ft (0.76 m). During the test, the south part of the basin remained stationary, while the north part was displaced to the north and west by large-stroke actuators to cause soil rupture and slip at the interface between the two parts of the test basin.

The 2D FE analyses were performed for 4-, 6-, 8-, 12-, 14-, and 16- in. (100-, 150-, 200-, 300-, 350-, and 400-mm, respectively)-diameter DI pipelines with TR- XTREME™ pipe joints using the test set-up shown in Figure 4.1, soil conditions described above, and 2.5 ft (0.76 m) of soil cover. All pipeline dimensions used in the FE simulations are consistent with those for thickness

Class 53 as provided by US Pipe (2103). The DI modulus as well as its proportional limit and yield stress are based on tensile test data reported by Wham and O'Rourke (2015) for commercial grade pipe.

4.2. Finite Element Simulations

Figure 4.2 shows a schematic of the 2D FE model of the pipeline response under strike-slip fault conditions, which was developed with the software ABAQUS (2014). The modeling procedure followed is in accordance with the Guidelines for Seismic Design of Oil and Gas Pipelines (ASCE, 1984). The pipeline model used for all pipe diameters was composed of 167 beam elements (type b33) and the soil resistance normal and parallel to the pipeline is simulated with 340 springs (type spring2). The beam elements follow a DI stress-strain relationship with Young's modulus, E , and Poisson's ratio, ν , equal to 27,000 ksi (186 GPa) and 0.375, respectively. The proportional limit and yield stress, σ_{prop} and σ_y , were 39.5 ksi (273 MPa) and 45.1 ksi (311 MPa), respectively.

Transverse bi-linear springs account for force vs. displacement relationships for lateral and longitudinal pipe movement. The transverse springs were calibrated based on numerical results for lateral force vs. displacement relationships presented by Jung et al. (2013). The longitudinal springs follow a bi-linear force vs. displacement relationship as suggested in the ASCE Guidelines. The maximum lateral and longitudinal forces are a function of soil properties, pipeline diameter and burial depth. For the purpose of these analyses, it was assumed that the pipeline is buried in partially saturated dense sand with dry unit weight, γ_{dry} , and moisture content, w , of 108 pcf and 4%, respectively. The ground displacements are imposed at the nodes of the transverse and longitudinal springs.

The joints were modeled with two independent nonlinear springs, one for force vs. displacement and one for moment vs. rotation. A third linear spring was used to model the shear force at each joint. For the 12-in. (300-mm) diameter pipelines, the results of the four-point bending tests, presented in Section 2, and joint tension tests, presented in Section 3, were used to model the moment vs. rotation and axial force vs. displacement relationships of the joints. The 6-in (150-mm)-diameter joints were modeled using the test results reported in Sections 3 and 5 of a previous report for US Pipe (Cornell University, 2015). The 6-in. (150-mm)- diameter joints are equipped with two restraining clips and are representative of the number of clips and their approximate locations around the joints of 4-, 6-, 8-, (100-, 150-, 200-mm, respectively)- diameter pipelines.

The 12-in. (300-mm) diameter joints are equipped with four restraining clips and are representative of the number of clips and their approximate locations around the joints of 12-, 14-, and 16- in. (300-, 350-, and 400-mm, respectively)-diameter pipelines.

The test results summarized in this report for 12-in. (300-mm)- diameter TR- XTREME™ joints compared to those summarized by Cornell University (2015) for 6-in. (150-mm)-diameter TR- XTREME™ joints show clear differences in the performance of joints with two clips relative to larger diameter joints with four clips. For example, the moment associated with the leakage of 6-in. (150-mm)-diameter joints with two clips (representative of smaller diameter joints) reach thresholds slightly higher than the proportional limit moment. In contrast, the moment associated with the leakage of 12-in. (300-mm)-diameter joints with four clips (representative of larger diameter joints) develop leakage at levels equivalent to 60 percent of the proportional limit moment. This lower level suggests that concentrated deformation at select clips is the cause for small rates of leakage at moments below the proportional limit. The axial load associated with pullout of the 6-in. (150-mm)-diameter joints (representative of smaller diameter joints) is caused by forces generated between the spigot bead and restraining clips that deform the spigot inward a sufficient distance to allow the bead to slip past the clips, with attendant loss of water pressure. This type of deformation does not occur in the 12-in. (300-mm) joints (representative of larger diameter joints) where four clips restrain spigot ovaling, with a corresponding increase in force and moment in the bell that eventually results in cracking of the bell.

For pipelines of different diameters a scaling procedure was followed to calculate the moment vs. rotation and force vs. pullout relationships for joints with different diameters. Pipelines of 4-in. and 8-in. (100- and 200-mm, respectively)-diameter were scaled with respect to the behavior exhibited by the 6 in. (150 mm) specimens, while pipelines of 14 in. and 16 in. (350 and 400 mm, respectively) were scaled relative to the results for the 12 in. (300 mm) specimen. The scaling parameter for moment is the proportional limit moment, M_{prop} , defined as $M_{prop} = \sigma_{prop}S$, for which σ_{prop} is the proportional stress at the limit of linear stress vs. strain behavior of DI and s is the sectional modulus of the pipe. The scaling parameter for axial force is the proportional limit force, P_{prop} , defined as $P_{prop} = \sigma_{prop}A$, for which σ_{prop} is the proportional limit stress and A is the cross-sectional area of the pipe.

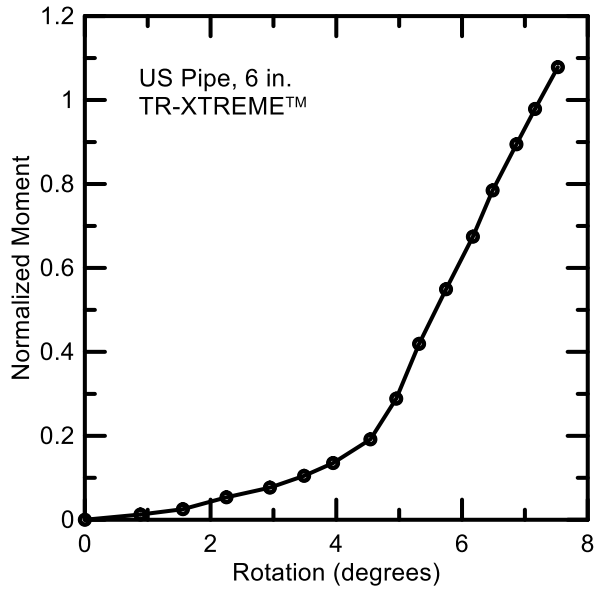


Figure 4.3. Normalized Moment vs. Rotation for 6 in. (150 mm) Pipe

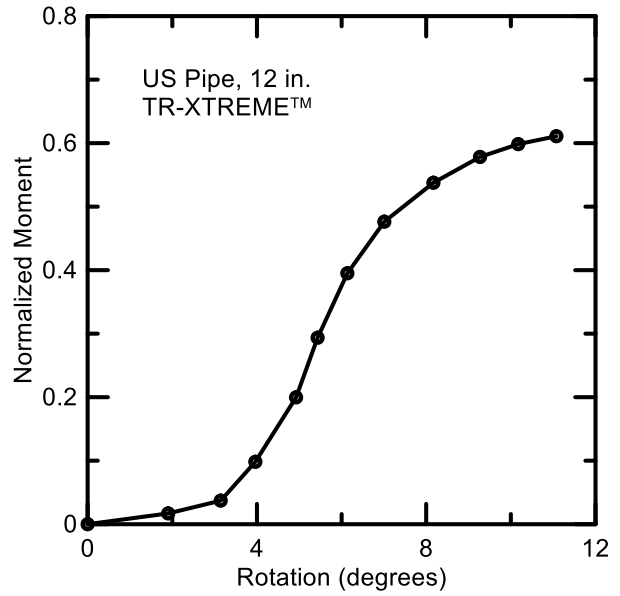


Figure 4.4. Normalized Moment vs. Rotation for 12 in. (300 mm) Pipe

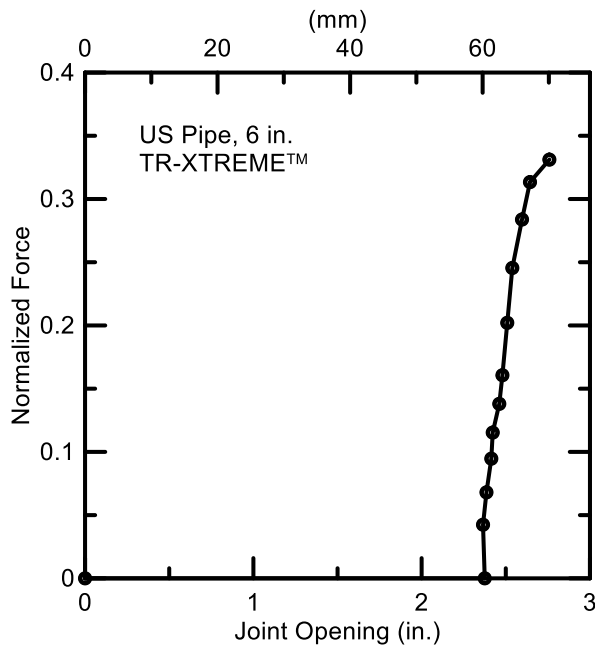


Figure 4.5. Normalized Joint Force vs. Joint Pullout for 6 in. (150 mm) Pipe

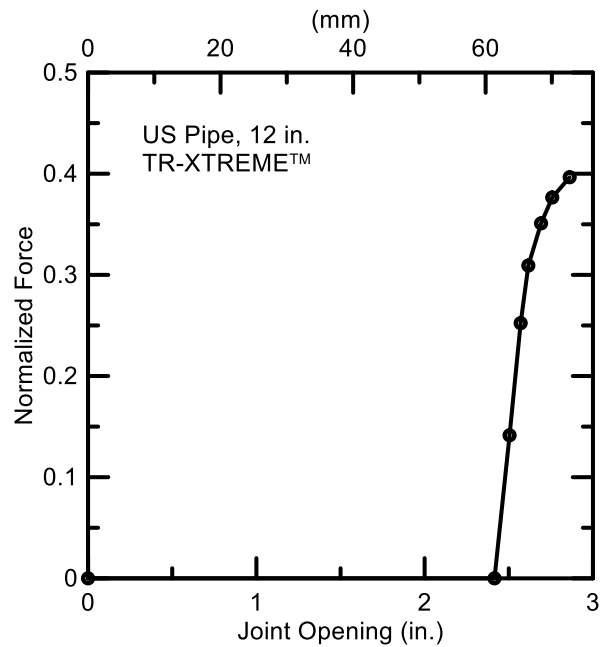


Figure 4.6. Normalized Joint Force vs. Joint Pullout for 12 in. (300 mm) Pipe

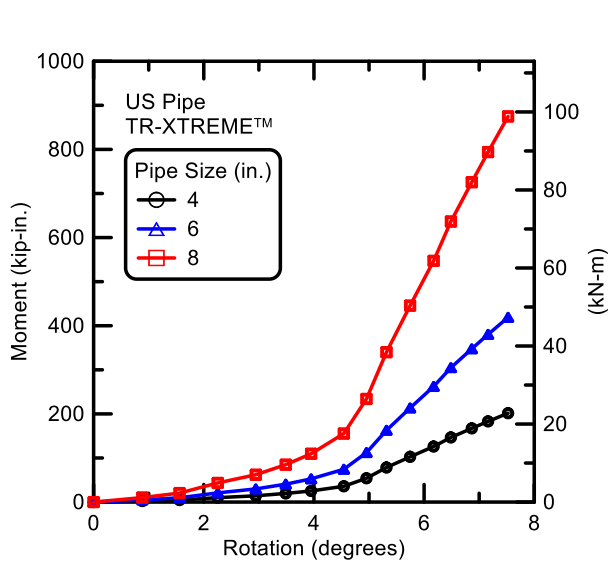


Figure 4.7. Analytical Moment vs. Rotation for 4, 6, and 8 in. (100, 150, and 200 mm) Pipes

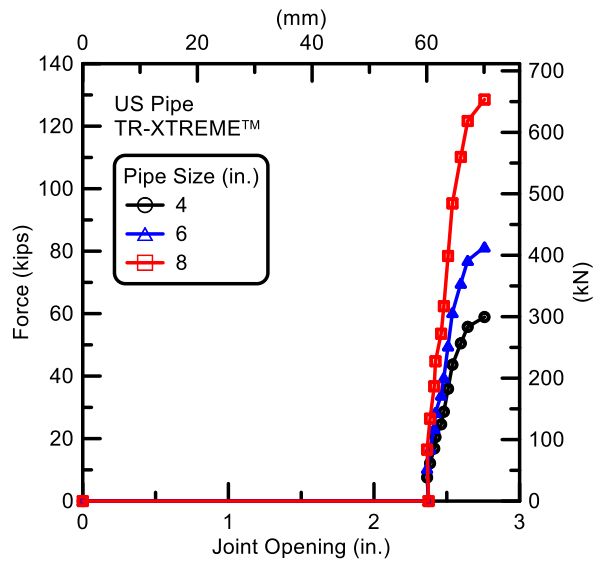


Figure 4.8. Analytical Joint Force vs. Joint Pullout for 4, 6, and 8 in. (100, 150, and 200 mm) Pipes

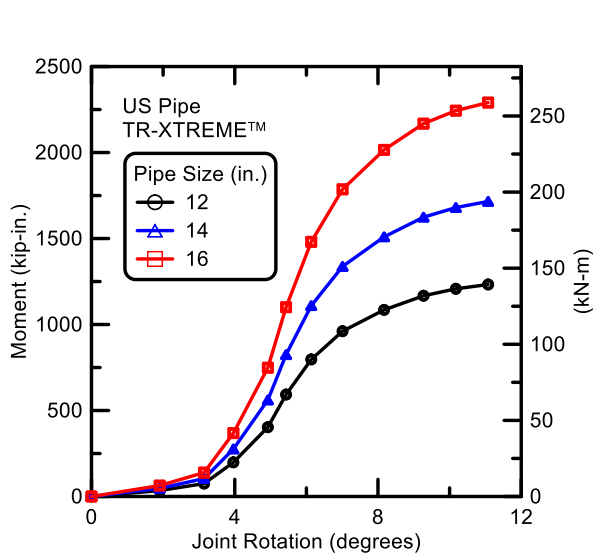


Figure 4.9. Analytical Moment vs. Rotation for 12, 14, and 16 in. (300, 350, and 400 mm) Pipes

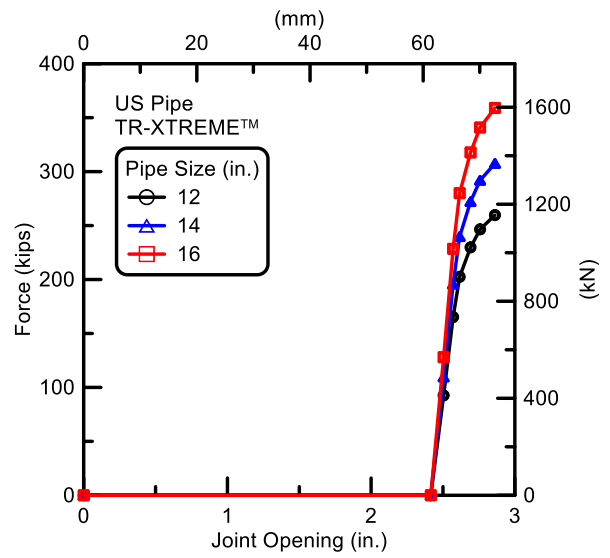


Figure 4.10. Analytical Joint Force vs. Joint Pullout for 12, 14, and 16 in. (300, 350, and 400 mm) Pipes

Figures 4.3 and 4.4 present the normalized joint moment, M/M_{prop} vs. rotation relationships for the 6 in. (150 mm) and 12 in. (300 mm) joint specimens, respectively. Figures 4.5 and 4.6 show the normalized joint axial force, P/P_{prop} vs. displacement relationships for the 6 in. (150 mm) and 12 in. (300 mm) joint specimens, respectively. These relationships are derived directly from the test results presented in this report, and by Cornell University (2015). Figures 4.7 and 4.8 show joint moment vs. rotation and joint force vs. displacement relationships that were used in the FE analyses of 4-, 6-, and 8-in. (100- 150- and 200-mm)-diameter pipelines. They were derived by multiplying the normalized moment vs. rotation and axial force vs. displacement relationships in Figures 4.3 and 4.5, respectively, with the corresponding M_{prop} and P_{prop} for each diameter pipeline. Figures 4.9 and 4.10 present the corresponding curves for 12, 14, and 16 in. (300, 350, and 400 mm) pipe diameters. They were derived in the same way as those for the smaller diameter joints.

4.3. Finite Element Simulation Results

Figures 4.11 and 4.12 present the FE simulation results for joint opening vs. fault displacement and joint rotation vs. fault displacement, respectively, for the 6 in. (150 mm) pipeline. These results agree very closely with the large-scale split basin test results provided by Cornell University (2015). Figures 4.13 and 4.14 present the FE simulation results for joint opening vs. fault displacement and joint rotation vs. fault displacement, respectively, for the 12 in. (300 mm) pipeline. These results also agree very closely with those for the 6 in. (150 mm) pipeline. In fact, the results for all diameter pipelines follow closely the trends in Figures 4.11 through 4.14. This similarity in response is expected because the pipeline joints are designed to accommodate abrupt ground displacement by joint rotation and axial joint slip in virtually the same way for each diameter pipeline, when subjected to similar fault rupture conditions. The FE simulation results confirm this similarity in performance.

Figures 4.15 and 4.16 present the FE simulation results for the axial strain for all pipeline sizes that were modeled corresponding to 9 in. (230 mm) and 18 in. (460 mm) of fault movement. At 9 in. (230 mm) of fault displacement, the axial movement of the pipeline was not of sufficient magnitude for the spigot bead to engage the restraining clips in all joints (see Figures 4.11 and 4.13). As a result only a relatively small axial force is mobilized in the pipeline, which is

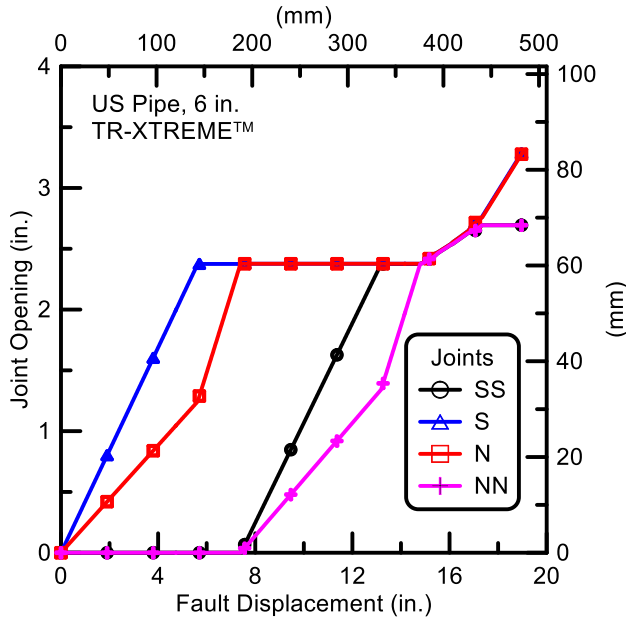


Figure 4.11. Joint Opening vs. Fault Displacement for 6 in. (150 mm) Pipes

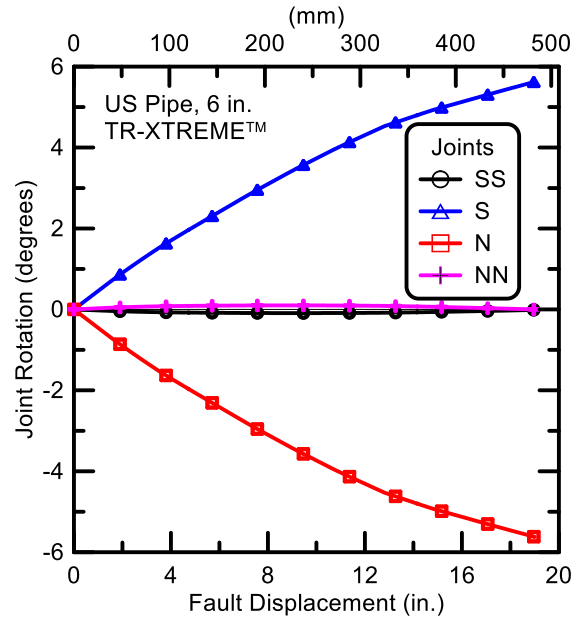


Figure 4.12. Joint Rotation vs. Fault Displacement for 6 in. (150 mm) Pipes

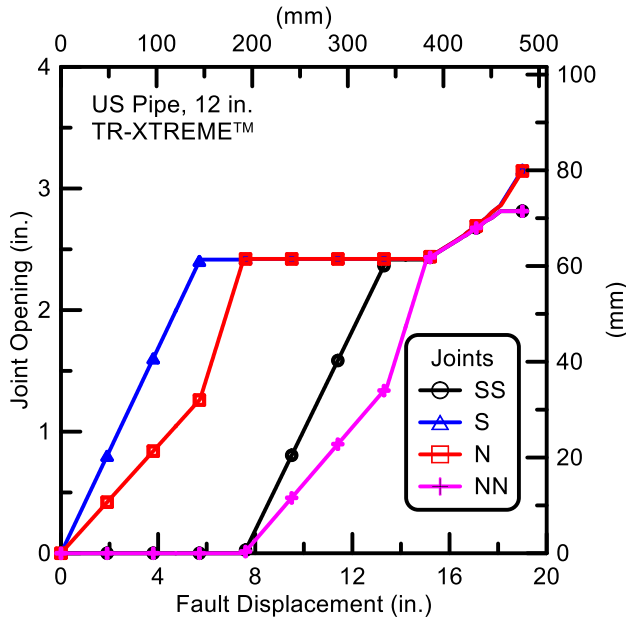


Figure 4.13. Joint Opening vs. Fault Displacement for 12 in. (300 mm) Pipes

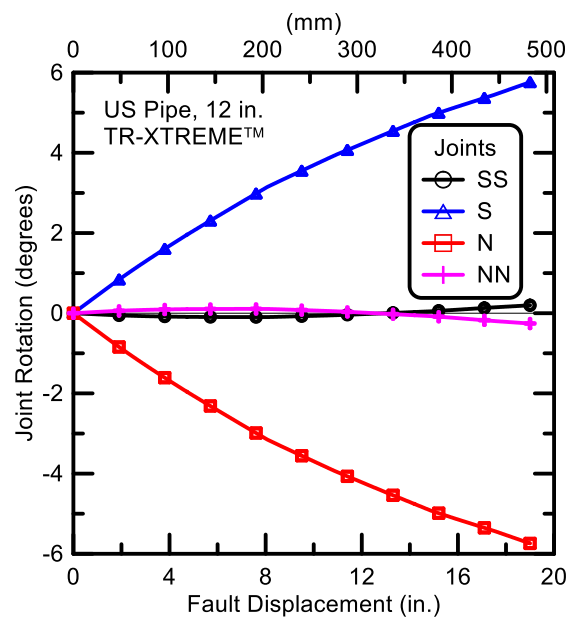


Figure 4.14. Joint Rotation vs. Fault Displacement for 12 in. (300 mm) Pipes

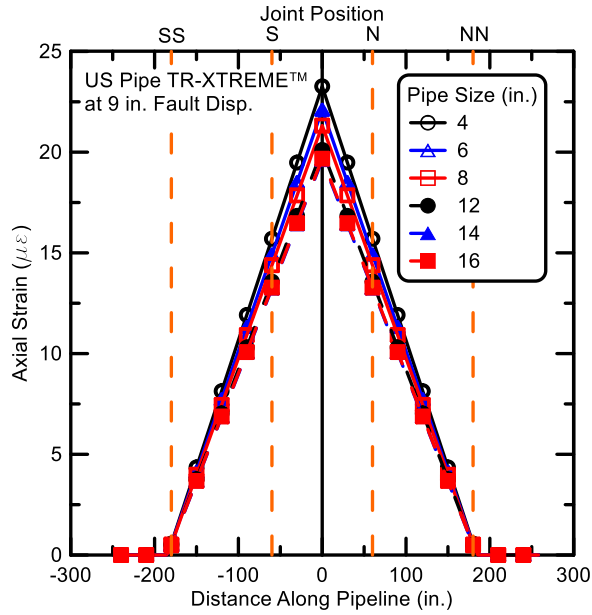


Figure 4.15. Axial Strain Comparisons at 9 in. (230 mm) of Fault Displacement

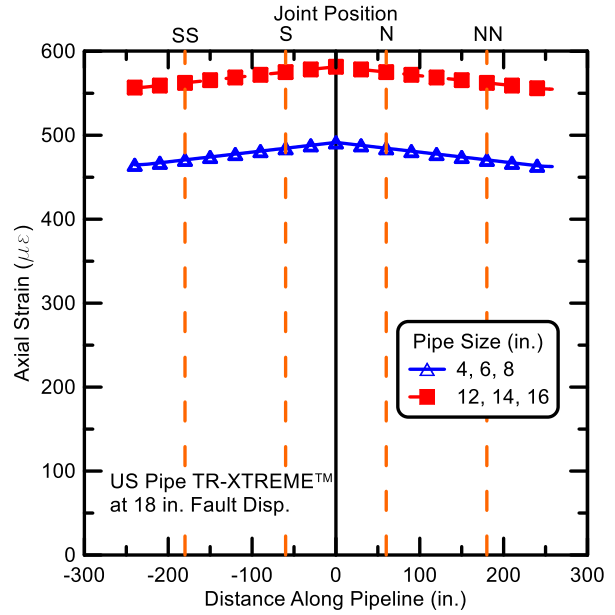


Figure 4.16. Axial Strain Comparisons at 18 in. (460 mm) of Fault Displacement

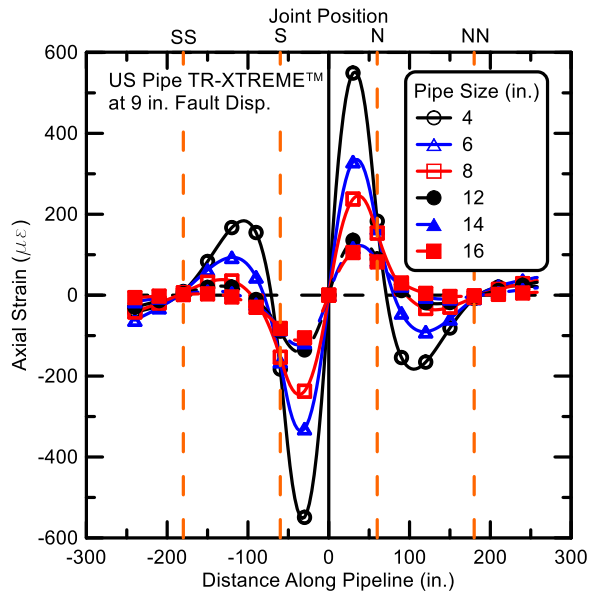


Figure 4.17. Bending Strain Comparisons at 9 in. (230 mm) of Fault Displacement

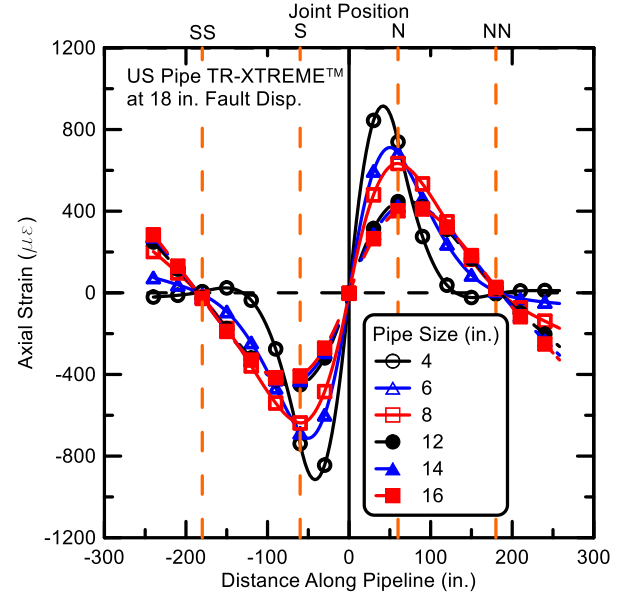


Figure 4.18. Bending Strain Comparisons at 18 in. (460 mm) of Fault Displacement

reflected in the small levels of axial strain for all pipe diameters. In contrast, at 18 in. (460 mm) of fault displacement the axial strains are over 20 times higher because all joints have slipped into firm contact between the spigot beads and the restraining clips and have mobilized nearly the full axially load capacity of the joints.

The axial strain response reflects the two types of axial force vs. displacement behavior for the smaller and larger diameter joints (see Figures 4.5 and 4.6). The axial strain distribution for each of the smaller and larger size categories is the same, but the axial forces are different within a given size category and can be computed for each diameter by multiplying the strain by the DI modulus and cross-sectional area of the pipe. For example, the maximum axial force in the 6-in. (150-mm)-diameter pipeline calculated from Figure 4.16 is approximately 82 kips (365 kN), which compares favorably with a maximum axial force of about 88 kips (390 kN) that was measured during the large-scale split basin test at Cornell (Cornell University, 2015).

The FE bending strains at various locations along the pipelines are plotted for 9 in. (230 mm) and 18 in. (460 mm) of fault movement in Figures 4.17 and 4.18, respectively. The bending strains were calculated as one half the difference between the springline strains. The bending strains increase in inverse proportion to pipe diameter. As the diameter increases, pipe segments between joints behave more like rigid pipe lengths so that the bending distortion decreases. The maximum bending strain in the 6-in. (150-mm)-diameter pipeline measured during the large-scale split basin test for 18 in. (460 mm) of fault displacement was nearly $700 \mu\epsilon$ (Cornell University, 2015), which compares well with the maximum strain of about $700 \mu\epsilon$ for the same size pipe and fault displacement as shown in Figure 4.18.

Table 4.1 summarizes the maximum strain and stress for all the FE simulations. The maximum strain is the maximum combination of axial and bending strains. In all cases the maximum stress is below the DI proportional limit stress, thus indicating linear stress vs. strain behavior for all pipe sizes.

4.4. Summary of Finite Element Simulations

Two-dimensional (2D) finite element (FE) analyses were performed for 4-, 6-, 8-, 12-, 14-, and 16- in. (100-, 150-, 200-, 300-, 350-, and 400-mm, respectively)-diameter DI pipelines with TR-XTREME™ joints using soil, pipe, and test dimensions consistent with the large-scale split basin

Table 4.1. Summary of Maximum Strains and Stresses for 4 to 16 in. (100 to 400 mm) Pipes

Pipe Nominal Diameter (in.)	Maximum Strain (micro)	Maximum Strain (%)	Maximum Stress (ksi)
4	1403	0.14	37.87
6	1198	0.12	32.36
8	1122	0.11	30.29
12	1030	0.10	27.82
14	1016	0.10	27.44
16	1001	0.10	27.01

1 in. = 25.4 mm; 1 ksi = 6.89 MPa

test performed at Cornell University for a 6-in. (150-mm)-diameter pipeline. All pipeline dimensions used in the FE simulations are consistent with those for thickness Class 53 available from US Pipe, and the DI material properties are consistent with those of pipe commercially available from US Pipe tested in previous Cornell research.

Based on the test results presented in this report, as well as previous results from large-scale Cornell tests, a scaling procedure was developed to calculate the moment vs. rotation and force vs. pullout relationships for joints with different diameters. Pipelines of 4 and 8 in. (100 mm and 200 mm, respectively) diameter were scaled with respect to the behavior exhibited by the 6 in. (150 mm) specimens, while pipelines of 14 and 16 in. (350 and 400 mm, respectively) were scaled relative to the results for the 12 in. (300 mm) specimen.

The FE simulation results for joint opening vs. fault displacement and joint rotation vs. fault displacement, respectively, are in close agreement for all sizes of pipe under study. They also agree very closely with those of the 6 in. (150 mm) pipeline used in the large-scale split basin test performed previously at Cornell University. The FE simulations show that the maximum axial strain distribution for each of the smaller and larger pipe size categories is the same, and is approximately 490 $\mu\epsilon$ and 580 $\mu\epsilon$ for 4-, 6- and 8-in. (100-, 150-, and 200-mm)-diameter pipelines and 12-, 14- and 16-in. (300-, 350-, and 400-mm)-diameter pipelines, respectively. The FE bending strains at various locations along the pipelines are provided for 9 in. (230 mm) and 18 in. (460 mm) of fault movement, and show that the bending strains increase in inverse proportion to pipe diameter. As the diameter increases, pipe segments between joints behave more like rigid pipe lengths so that the bending distortion decreases. In all cases the maximum stress from the FE

results is below the DI proportional limit stress, thus indicating linear stress vs. strain behavior for all pipe sizes. The maximum axial and bending strains from the FE simulations for 6-in. (150-mm)-diameter pipe compare well with the measurements of maximum axial and bending strains obtained during the previous large-scale split basin test at Cornell, thus providing confidence in the FE results.

Section 5

Summary

US Pipe has developed a hazard resistant ductile iron (DI) pipe joint, called the TR-XTREME™ joint. Sections of 12-in. (300-mm)- diameter pipes with the new joints were tested at Cornell University to 1) evaluate the bending resistance and moment-rotation relationship of the joint for two positions of the locking clip segments, and 2) determine the capacity of the joint in direct tension. In addition, finite element (FE) analyses were performed for 4- through 16-in. (100-through 400-mm)-diameter pipelines with TR-XTREME™ joints to show how these sizes of pipelines would respond to large-scale split-basin tests, similar to the one conducted on a pipeline with 6-in. (150-mm)- diameter joints (Cornell University, 2015).

It should be noted that the term “rotation” in this report is equivalent to “deflection” as used commonly in the field and commercial pipeline information. Test results are summarized for bending and direct tension tests, as well FE simulations under the headings that follow.

5.1. Bending Test Results

Four-point bending tests on 12-in. (300-mm)-diameter pipes were performed to evaluate the moment vs. rotation relationships of the TR-XTREME™ joints when the locking clips were at the 3 and 9 o’clock positions (Test A) and the 12 and 6 o’clock positions (Test B). First leakage was observed at a moment of 565 kip-in. (63.7 kN-m) and an average joint rotation of 6.5 degrees for Test A. The first leakage stopped after depressurization and did not occur again until a rotation of 10.3 degrees under 80 psi (552 kPa) internal pressure. The first leakage of Test B was detected at an applied moment of 350 kip-in. (39.4 kN-m) and 4.8 degrees of average joint rotation. The average rotation at first leakage for the two tests is 5.6 degrees.

The joints were able to sustain substantially higher moment and rotations beyond moment and rotation at first leakage. The maximum leakage of Test A occurred at an applied moment of 1770 kip-in. (200 kN-m) and an average joint rotation of 15.9 degrees. The test was terminated without significant damage or dislocation at the joint. The maximum leakage of Test B was observed at an applied moment of 1240 kip-in. (140 kN-m) and an average joint rotation of 11 degrees. The test was terminated when the invert restraining clips slipped out of the joint.

The moment vs. rotation relationships for the two tests are similar to a rotation of approximately 10 degrees. Higher moments were mobilized at smaller rotation angles when the clips were positioned closer to the 12 and 6 o'clock positions in alignment with the applied load. The maximum moments developed in both tests were well below both the proportional limit moment, M_{prop} , and the yield moment, M_{yield} .

5.2. Direct Joint Tension

Two tension tests were performed on the 12-in. (300-mm)-diameter US Pipe TR-XTREME™ joints. Both tests began with the spigot fully inserted in the bell. As the pipe was pressurized, the spigot was displaced from the bell seat at approximately 6 psi (41 kPa) internal pressure. The slip was 2.43 in. (61.7 mm) and 2.27 in. (57.7 mm) before the weld bead became engaged with the restraining clips for Tests 1 and 2, respectively. Tests 1 and 2 reached a maximum force of 220 kips (977 kN) at 2.83 in. (71.9 mm) of axial displacement and a maximum axial load of 259 kips (1153 kN) at 2.92 in. (74.2 mm) of joint displacement, respectively. The onset of leakage is caused by forces generated between the spigot bead and restraining clips that crack the bell circumferentially. The joints began to leak at openings of 2.84 and 2.99 in. (72.1 mm and 75.9 mm) for Tests 1 and 2, respectively. After the weld bead on the spigot made contact with the clips, an additional movement between 0.4 and 0.7 in. (10 mm and 18 mm) was required to generate leakage at the joint.

The maximum axial load of 259 kips (1150 kN) in Test 2 is more representative of the axial load capacity of the 12-in. (300-mm)-diameter US Pipe TR- XTREME™ joint and should be used for the best estimate of maximum load capacity for direct axial loading. The maximum axial load caused cracking of the pipe bell. Given an initial slip of 2.27 in. (57.7 mm) to engage contact between the spigot bead and restraining clips, an additional movement of approximately 0.65 in. (16.5 mm) was required to initiate cracking of the bell and leakage at the joint.

5.3. Finite Element Simulations

Two-dimensional (2D) finite element (FE) analyses were performed for 4-, 6-, 8-, 12-, 14-, and 16- in. (100-, 150-, 200-, 300-, 350-, and 400-mm, respectively)-diameter DI pipelines with TR-XTREME™ joints using soil, pipe, and test dimensions consistent with the large-scale split basin test performed at Cornell University for a 6-in. (150-mm) diameter pipeline. All pipeline

dimensions used in the FE simulations are consistent with those for thickness class 53 available from US Pipe, and the DI material properties are consistent with those of pipe commercially available from US Pipe tested in previous Cornell research.

Based on the test results presented in this report as well as previous results from large-scale Cornell tests, a scaling procedure was developed to calculate the moment vs. rotation and force vs. pullout relationships for joints with different diameters. Pipelines of 4-in. and 8-in. (100-mm and 200-mm, respectively) diameter were scaled with respect to the behavior exhibited by the 6-in. (150-mm) specimens, while pipelines of 14-in. and 16-in. (350-mm and 400-mm, respectively) were scaled relative to the results for the 12-in. (300-mm) specimen.

The FE simulation results for joint opening vs. fault displacement and joint rotation vs. fault displacement, respectively, are in close agreement for all sizes of pipe under study. They also agree very closely with those of the 6-in. (150-mm) pipeline used in the large-scale split basin test performed previously at Cornell University. The FE simulations show that the maximum axial strain distribution for each of the smaller and larger pipe size categories is the same, and is approximately $490 \mu\epsilon$ and $580 \mu\epsilon$ for 4-in., 6-in. and 8-in. (100-mm, 150-mm, and 200-mm)-diameter pipelines and 12-in., 14-in. and 16-in. (300-mm, 350-mm, and 400-mm)-diameter pipelines, respectively. The FE bending strains at various locations along the pipelines are provided for 9-in. (230-mm) and 18-in. (460-mm) of fault movement, and show that the bending strains increase in inverse proportion to pipe diameter. As the diameter increases, pipe segments between joints behave more like rigid pipe lengths so that the bending distortion decreases. In all cases the maximum stress from the FE results is below the DI proportional limit stress, thus indicating linear stress vs. strain behavior for all pipe sizes. The maximum axial and bending strains from the FE simulations for 6-in. (150-mm)-diameter pipe compare well with the measurements of maximum axial and bending strains obtained during the previous large-scale split basin test at Cornell, thus providing confidence in the FE results.

5.4. Significance of Large-Scale Test and Finite Element Simulation Results

The test results and FE simulations presented in this work corroborate the results of previous testing and reporting by Cornell (Cornell University, 2015). It should be recognized that the amount of tensile strain that can be accommodated with pipelines with TR-XTREME™ joints will

depend on the axial separation between the pipeline joints. The pipeline used in the large-scale split-basin test (Cornell University, 2015) was able to accommodate 12.2 in. (206 mm) of axial extension, corresponding to an average tensile strain of 2.61% along the pipeline. The FE results presented in this report show similar performance for all sizes of pipelines between 4 in. (100 mm) and 16 in. (400 mm). Such extension is large enough to accommodate the great majority (over 99%) of liquefaction-induced lateral ground strains measured by high resolution LiDAR after each of four major earthquakes during the recent Canterbury Earthquake Sequence (CES) in Christchurch, NZ (O'Rourke et al., 2014). These high resolution LiDAR measurements for the first time provide a comprehensive basis for quantifying ground strains caused by liquefaction on a regional basis. To put the CES ground strains in perspective, liquefaction-induced ground deformation measured in Christchurch exceed those documented in San Francisco during the 1989 Loma Prieta earthquake (e.g., O'Rourke and Pease, 1997; Pease and O'Rourke, 1997) and in the San Fernando Valley during the 1994 Northridge earthquake (e.g., O'Rourke, 1998). They are comparable to the levels of most severe liquefaction-induced ground deformation documented for the 1906 San Francisco earthquake, which caused extensive damage to the San Francisco water distribution system (e.g. O'Rourke and Pease, 1997; O'Rourke et al., 2006).

The test results and FE simulations presented in this report confirm that the TR-XTREME™ joints are able to sustain without leakage large levels of ground deformation through axial displacement and rotation. The test results are directly applicable to the performance of nominal 4-in. (100-mm) to 16-in. (400-mm)-diameter US Pipe DI pipelines with TR-XTREME™ joints.

References

- ABAQUS, (2014) “Theory Manual of ABAQUS,” ABAQUS, Inc., Providence, RI.
- ASCE. (1984) “Guidelines for the Seismic Design of Oil and Gas Pipeline Systems”, Committee on Gas and Liquid Fuel Lifelines, ASCE, Reston, VA.
- Cornell University (2015) “Hazard Resilience Testing of US Pipe Ductile Iron TR-XTREME™ Pipe Joints” report prepared for US Pipe by Cornell University, February, 2015.
- Jung, J., O’Rourke, T.D., and Olson, N. A. (2013) “Lateral Soil-Pipe Interaction in Dry and Partially Saturated Sand” Journal of Geotechnical and GeoEnvironmental Engineering, ASCE, Vol. 139, No. 12, pp. 2028-2036.
- O’Rourke, T.D. (1998). “An Overview of Geotechnical and Lifeline Earthquake Engineering”, Geotechnical Special Publication No. 75, ASCE, Reston, VA, Proceedings of Geotechnical Earthquake Engineering and Soil Dynamics Conference, Seattle, WA, Aug. 1998, Vol 2, pp.1392-1426.
- O’Rourke, T.D. and J.W. Pease (1997). “Mapping Liquefiable Layer Thickness for Seismic Hazard Assessment”, Journal of Geotechnical Engineering, ASCE, New York, NY, Vol. 123, No.1, Jan., pp. 46-56.
- O’Rourke, T.D., A. Bonneau, J. Pease, P. Shi, and Y. Wang (2006). “Liquefaction Ground Failures in San Francisco” Earthquake Spectra, EERI, Oakland, CA, Special 1906 San Francisco Earthquake Vol. 22, No. 52, Apr., pp. 691-6112.
- O’Rourke, T.D., Jeon, S-S., Toprak, S., Cubrinovski, M., Hughes, M., van Ballegooy, S., and Bouziou, D. (2014) “Earthquake Response of Underground Pipeline Networks in Christchurch, NZ”, Earthquake Spectra, EERI, Vol. 30, No.1, pp. 183-204.
- Pease, J.W. and T.D. O’Rourke (1997), “Seismic Response of Liquefaction Sites”, Journal of Geotechnical Engineering, ASCE, New York, NY, Vol. 123, No. 1, January, pp. 37-45.
- U.S. Pipe (2013) “TR Flex™ Retrained Joint Ductile Iron Pipe and Fittings”, 2013 Edition, US Pipe.
- Wham, B.P. and T.D. O’Rourke (2015) “Jointed Pipeline Response to Large Ground Deformation”, Journal of Pipeline Systems Engineering and Practice, ASCE, (in press.)